Image Registration and Image Segmentation for Image-Guided Radiotherapy of Prostate Cancer

Image Registration and Image Segmentation for Image-Guided Radiotherapy of Prostate Cancer

PhD Thesis by

Anne Sofie Korsager

Department of Health Science and Technology
Aalborg University, Denmark

River Publishers

ISBN 978-87-93237-29-2 (Ebook)

Published, sold and distributed by:
River Publishers
Niels Jernes Vej 10
9220 Aalborg Ø
Denmark

Tel.: +45369953197
www.riverpublishers.com

PhD thesis:
Image Registration and Image Segmentation for Image-Guided Radiotherapy of Prostate Cancer

PhD student:
Anne Sofie Korsager

Supervisors:
Associate Professor, PhD, Lasse Riis Østergaard,
Department of Health Science and Technology, Aalborg University

Associate Professor, PhD, Medical Physicist, Jesper Carl,
Department of Medical Physics, Oncology, Aalborg University Hospital

List of publications:

- Anne Sofie Korsager, Jesper Carl and Lasse Riis Østergaard. MR-CT registration using a Ni-Ti prostate stent in image-guided radiotherapy of prostate cancer. Medical Physics, Vol. 40, No. 6, 2013.
- Anne Sofie Korsager, Jesper Carl and Lasse Riis Østergaard. Comparison of manual and automatic MR-CT image registration for image-guided radiotherapy of prostate cancer. Submitted.
- Anne Sofie Korsager, Ulrik Landberg Stephansen, Jesper Carl and Lasse Riis Østergaard. The use of an active appearance model for automated prostate segmentation in magnetic resonance. Acta Oncologica. Vol. 52. No. 7, 2013
- Anne Sofie Korsager, Valerio Fortunati, Fedde van der Lijn, Jesper Carl, Wiro Niessen, Lasse Riis Østergaard, Theo van Walsum. The use of atlas registration and graph cuts for prostate segmentation in magnetic resonance images. Submitted.

In addition, the following work was published during the PhD:

- Anne Sofie Korsager, Jesper Carl and Lasse Riis Østergaard. MR-CT registration in image-guided radiotherapy of prostate cancer using a Ni-Ti prostate stent. Radiotherapy & Oncology, Vol. 103, Nr. Suppl. 1, p. S535-S536, ESTRO31 2012.
- Ulrik Landberg Stephansen, Ronnie W. Horup, Mikkel Gram, Jens Tranholm Olesen, Jesper Carl, Anne Sofie Korsager, Lasse Riis Østergaard. Airway tree segmentation for optimal stent placement in image-guided radiotherapy. The Fourth International Workshop on Pulmonary Image Analysis, 2011.

Preface and Acknowledgements

This thesis has been submitted for assessment in partial fulfillment of the PhD degree at Department of Health Science and Technology, Aalborg University. The thesis presents the work performed during my PhD study in the period February 2011-May 2014, under the supervision of Lasse Riis Østergaard, Aalborg University, and Jesper Carl, Aalborg University Hospital. The PhD study was performed in the Medical Informatics Group, Department of Health Science and Technology, Aalborg University, Denmark.

The work was carried out in collaboration with the Department of Medical Physics, Oncology, Aalborg University Hospital, including exchange of the materials used in all studies. Also, a part of my PhD was carried out at the Biomedical Imaging Group Rotterdam, Erasmus MC, Nederlands, under the supervision of Theo van Walsum.

The content of the thesis is based on four papers written during the PhD period. In addition to the papers, an introduction to the research area and a brief overview of the literature is given as well as a discussion of the work presented in this thesis and future work.

A number of people have provided their knowledge and support to my PhD study, and I wish to express my gratitude to them for contributing to this work.

First, my supervisors Jesper Carl and Lasse Riis Østergaard for their supervision, support, and confidence in me. Thanks for the numerous discussions and thoughtful criticism which substantially improved the quality of my work. I would also like to thank the people at the Department of Medical Physics, Aalborg University Hospital, for their kindness and help. Thanks also goes to Ulrik Landberg Stephansen for helping me getting started with the appearance modeling and the software needed for that.

During my PhD I had the opportunity to visit the Biomedical Imaging Group Rotterdam, Department of Medical Informatics and Radiology, Erasmus MC. I am thankful for the invitation and the supervision from Theo van Walsum and to all the inspiring and helpful people in the Biomedical Imaging Group Rotterdam, especially Wiro Niessen, Fedde van der Lijn, and Valerio Fortunati for their suggestions for improvements and help with the methodology and software.

I would also like to thank current and former colleagues from the Medical Informatics Group at the Department of Health Science and Technology for an inspiring working environment and enjoyable coffee breaks. A special thanks goes to Kirstine Rosenbeck Gøeg, Zeinab Mahmoudi, and Ask Schou Jensen for keeping me company at the office.

Finally, I wish to thank my fiends and family and last but not least my husband Kasper for his absolutely unbelievable patience and support.

Anne Sofie Korsager
Aalborg University, November 23, 2014

English Abstract

Medical imaging plays a key role in treatment of various cancer types and in particular in image-guided radiotherapy (IGRT) and can be used in all stages of the radiotherapy treatment including accurate target delineation and radiation dose calculations in the planning of IGRT. Magnetic resonance (MR) imaging is often used for accurate soft-tissue delineation and computed tomography (CT) images are used for radiation dose calculations. The accurate target delineation together with multimodal imaging may enable a smaller radiation field. This is important in IGRT as it enables a high radiation dose to the target and minimizes the radiation dose to the surrounding healthy tissue, which results in an improved treatment outcome with lower toxicity and reduced side-effects.

The use of multimodal imaging requires alignment of MR and CT in order to map the target delineation in MR to CT for dose calculations. The target delineation and the image alignment are today widely performed manually and are therefore time-consuming, labor-intensive, and prone to observer variations. The target for radiation is extended to include healthy tissue to ensure that the tumor is always radiated during treatment as a consequence of the observer variation together with other uncertainties.

The thesis seeks to address these challenges in the planning of radiotherapy of prostate cancer. Prostate cancer is a cancer type where the treatment highly benefits from the use of IGRT and multimodal imaging. The prostate is delineated as the target in MR because of the good soft-tissue visualization in MR and a following image alignment enables dose calculations based on CT. At Aalborg University Hospital a newly developed removable Ni-Ti prostate stent is implanted into the prostate gland and is used as a fiducial marker to achieve an accurate alignment of the prostate in MR and CT. The first part of the thesis focuses on automatic image alignment using voxel similarity and on a comparison of the automatic approach with the current clinical approach. The second part focuses on automatic target delineation. Two automatic approaches for target delineation in MR using both voxel intensities and knowledge about the shape are developed and validated.

The approaches presented are expected be adaptable to target delineation and image alignment of other soft-tissue organs.

Dansk resumé (Danish Abstract)

Medicinske billeder er et væsentligt redskab i behandling af kræft og særligt i billedvejledt strålebehandling, hvor billederne kan blive anvendt i alle faser af strålebehandlingen f.eks. i planlægningsfasen for at indtegne strålefeltet præcist og til at udregne dosisfordelingen i kroppen. Magnetisk resonans (MR) billeder er ofte brugt til at indtegne kroppens bløddele og computertomografi (CT) bruges til at beregne fordelingen af stråledosis i kroppen. En mere præcise indtegning af bløddele sammen med multimodale billeder kan give et mindre strålefelt. Det er vigtigt i billedvejledt strålebehandling, fordi det kan muliggøre en høj bestråling af tumor, mens det samtidig kan minimere bestråling af det omkringliggende raske væv. Den mere præcise behandling betyder et forbedret behandlingsresultat med en reduceret toksicitet af rask væv og færre bivirkinger og komplikationer som følge af behandlingen.

Billedregistering af MR og CT er nødvendig ved brug af multimodale billeder for at kunne overføre indtegningen af strålefeltet fra MR til CT for derefter at kunne beregne dosisfordelingen. Både indtegningen af strålefeltet og registeringen af MR og CT er i dag hovedsageligt udført manuelt, hvilket er tids- og arbejdskrævende samt tilbøjelig til at tilføje observatørvariationer i planlægningen af strålebehandlingen. Som følge af bl.a. observatørvariationer bliver strålefeltet udvidet, så det også indbefatter rask væv for at sikre, at tumor bliver bestrålet.

Denne afhandling omhandler disse udfordringer i forbindelse med planlægning af strålebehandling af prostatakræft. Prostatakræft er en kræfttype, hvor behandlingen har en stor fordel af billedvejledt strålebehandling og multimodale billeder. Prostatakirtlen er indtegnet som strålefeltet i MR pga. MRs gode visualisering af bløddele og en efterfølgende billedregistrering muliggør beregningen af dosisfordelingen vha. CT. For at kunne opnå en præcis billedregistrering af MR og CT bruger Aalborg Universitetshospital en nyudviklet prostatastent, der implanteres i prostatakirtlen, som markør. Afhandlingens første del fokuserer på automatisk intensitetsbaseret billedregistrering af MR og CT og på en sammenligning af den automatiske billedregistrering og den nuværende anvendte manuelle billedregistrering. Afhandlingens anden del fokuserer på automatisk indtegning af prostata som strålefeltet i MR ved brug af to forskellige metoder. To metoder, der begge bruger billedintensiteter og en viden om prostatas form, er udviklet og valideret i forhold til manuelle indtegninger af prostata.

De præsenterede metoder forventes at kunne tilpasses til registering og indtegning af andre bløddelsstrukturer.

Contents

Nomenclature

AAM	Active appearance models
AB	Atlas-based segmentation
$AB + IM$	Method combining atlas registration, intensity modeling, and graph cuts
CT	Computed tomography
CTV	Clinical target volume
DSC	Dice similarity coefficient
GTV	Gross tumor volume
$IGRT$	Image-guided radiotherapy
$IMRT$	Intensity-modulated radiotherapy
MR	Magnetic resonance
MSD	Mean surface distance
PCA	Principal component analysis
PTV	Planning target volume

1 Introduction

1.1 Background

Radiotherapy plays a key role in the treatment of cancer. The goals of the treatment are to shrink the tumors and kill cancer cells to cure the cancer patient with a minimum of side effects. An important step to obtain a better treatment is to improve the accuracy of the radiation field so that the target for radiation gets a maximal radiation dose and, at the same time, to reduce the exposure of surrounding healthy tissue. Advances in the planning of radiotherapy and treatment have focused on sparing the healthy tissue while allowing the same or higher radiation dose to the target. [1]

Advances in medical imaging have been essential for this development and image-guided radiotherapy (IGRT) is now often used to treat cancer. IGRT enables a visualization of the target and the surrounding healthy tissue so that an accurate target definition is possible, which can reduce the radiation dose to the surrounding healthy tissue if the radiation beam is shaped to fit the target. Furthermore, IGRT uses imaging in the treatment room for patient setup in the treatment system, which also decreases the uncertainties in the treatment. Computed tomography (CT) is used for planning radiotherapy and dose calculations and is thus referred to as the planning CT. Other imaging modalities can be aligned with CT to provide a better target visualization e.g. the good soft-tissue visualization in magnetic resonance (MR) and positron emission tomography to add functional information about the tumor. During treatment the target can be localized, potential target movement can be tracked, and the patient can be accurately aligned with the treatment system. All this is based on image information. [2, 3] A further advantage of IGRT is that it encourages the use of intensity-modulated radiotherapy (IMRT) planning, which offers a highly conformal 3D radiation field. The advantages of IMRT include a concave dose distribution and steep dose gradients. This has improved the therapeutic ratio by facilitating dose escalation and, at the same time, sparing the healthy tissue compared with conventional radiotherapy because IMRT allows a modulation of the intensity of each radiation beam. [4, 5] The risk of using IMRT and a highly conformal radiation field is geometrical misses because of the sharp edges between the radiation field and the surrounding tissue. This stresses the importance of accurate treatment planning. [4]

The advances in IGRT and IMRT are challenged due to several uncertainties and sources of errors in the planning of radiotherapy and the treatment, which reduce the radiation dose to the target and increase the radiation dose to the healthy tissue. The uncertainties include errors in the definition of the target, movement of the target, setup errors, visualization uncertainties, and the use of different modalities because an alignment is needed. Therefore, margins are added to the tumor and new volumes are used to plan the treatment. Typically, three volumes are used, the gross tumor volume (GTV), the clinical target volume (CTV), and the planning target volume (PTV), see Figure 1.1 for an example of the three volumes. The GTV (solid) is the part of the tumor that is visible. The CTV (dashed) includes the GTV and the subclinical and microscopic anatomical spread patterns, and it is generated by adding a predefined margin to the GTV based on clini-

cal and pathological experience. The PTV (dotted) consists of predefined safety margins added to the CTV to account for the uncertainties in the planning process or treatment e.g. tumor movement. A side-effect of the large margins added to the tumor is that large areas of healthy tissue adjacent to the target are included into the radiation volume. [6]

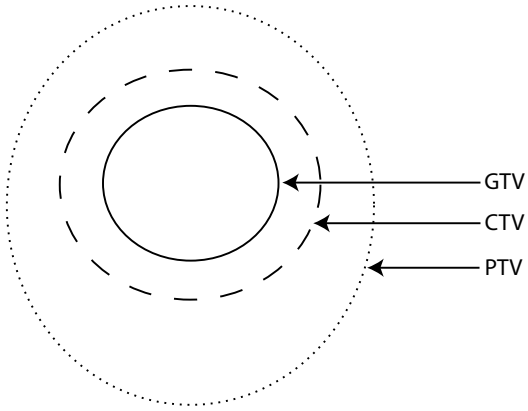

Figure 1.1: The three margins typically used for planning IGRT. Solid line: the GTV, dashed line: the CTV, dotted line: the PTV.

Studies which have compared IMRT and conventional 3D conformal radiotherapy have showed a reduced acute and late radiation-induced side-effects using IMRT. [4] The reductions in acute and late toxicities are particular important in radiotherapy of prostate cancer because the survival rates of prostate cancer are better than for most other cancer types and many patients will therefore live for years with the side-effects of their treatment. Critical and healthy structures such as the small bowel, the rectum, and the bladder risk to be damaged in radiotherapy of prostate cancer. Increased toxicity and damage may result in pain, bleeding, incontinence, nocturia, etc. [7]. These side-effects are a limiting factor for the radiation dose even though dose escalation has shown to increase the biochemical control of the treatment [8, 9, 10].

CT is the standard imaging modality for planning of IGRT of prostate cancer. CT provides a good spatial accuracy and provides the electron density data needed for the dose planning to calculate the attenuation of the radiation dose. A disadvantage of CT is the poor soft-tissue visualization. T_2-weighted MR imaging is, on the other hand, superior to CT in terms of soft-tissue visualization, and is therefore the preferred choice for delineation of the CTV. Fig. 1.2 shows the visualization of the prostate in corresponding CT and MR images, which illustrates that there is a lack for distinction between the prostate and the surrounding tissue due to the poor soft-tissue visualization in the CT image. A number of studies e.g. by Sannazzari et al. [11], Hentschel et al. [12], and Rasch et al. [13] have compared MR and CT for prostate delineation and demonstrated that the mean prostate volume was 1.34, 1.35 and 1.4 times larger in CT compared with MR, respectively. An overestimation of 34% of the CTV delineation on CT compared with MR corresponds to an almost 5 mm larger CTV radius than if MR was used [11]. In addition to the improved accuracy in target delineation on MR, the interobserver variation is reduced in MR compared with CT [14]. Brabandere et al. [15] investigated interobserver

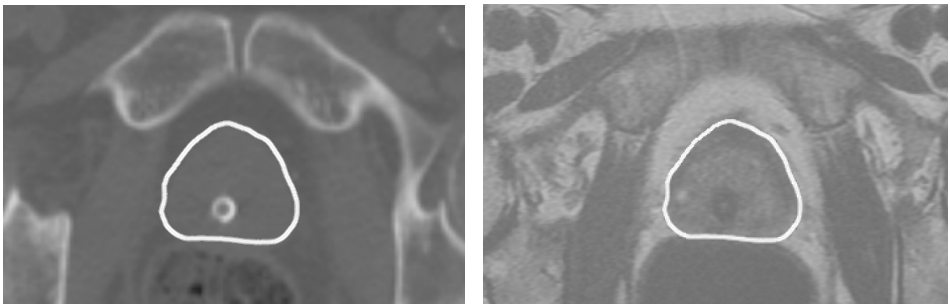

Figure 1.2: Corresponding CT (left) and MR (right) scan from the same patient, where the manual CTV contour is superimposed. The prostate (white contour) is clearly better visualized in MR compared with CT.

variation using either CT or MR for prostate delineation. The interobserver variation was, as expected, largest on CT with 23.4% in variation compared with 17.1% using MR. The authors found the variation using MR for delineation unexpectedly large but concluded that the variation was mainly caused by a difference in agreement of the location of the prostate boundary and because some of the authors seemed to include a margin to the CTV even though only the prostate gland should be delineated as the CTV. Nevertheless, the interobserver variation associated with manual delineation is still an unsolved problem [16, 17].

Spatial alignment, also called image registration, of MR and CT is common in IGRT of prostate cancer for adding an accurate target delineation in MR to the CT for dose planning. [12] Today this is primarily performed by selecting corresponding anatomical landmarks in MR and CT to determine the spatial alignment between the imaging modalities. A well-known uncertainty related to the spatial alignment of MR and CT for radiotherapy planning of prostate cancer is the prostate movement. The prostate movement results in different positions and orientations of the prostate relative to the pelvic bones and skin markers [18, 19, 20] and is a limiting factor in the achievement of reduced margins added to CTV. An alignment of the bones can reduce the size of the CTV because MR can be used for delineation, however, a registration based on the pelvic bones does not change the size of the margin added to the CTV to define the PTV. [14] Consequently, a local registration of the prostate is needed to account for the translational and rotational movement of the prostate relative to the pelvic bones. A MR-CT registration of the prostate to limit the influence from the pelvic bones can be achieved using intraprostatic fiducial markers implanted into the prostate gland as a surrogate for the prostate. Fiducial markers are needed as the difference in image contrast in MR and CT makes it difficult to identify common structures within the prostate. The fiducial markers can be used for verification of the prostate location and thereby account for the prostate movement relative to the pelvic bones. A frequently used fiducial marker are gold markers implanted into the prostate gland [21]. As an alternative to the gold markers a removable Ni-Ti prostate stent [22] has been developed and is now used at Aalborg University Hospital. The prostate stent has several advantages compared with gold markers e.g. that it causes less artifacts in CT, is clearly visible in MR, and can be perceived as a 3D object [23, 24]. Fig. 1.3

illustrates the prostate stent in CT (left) and MR (right).

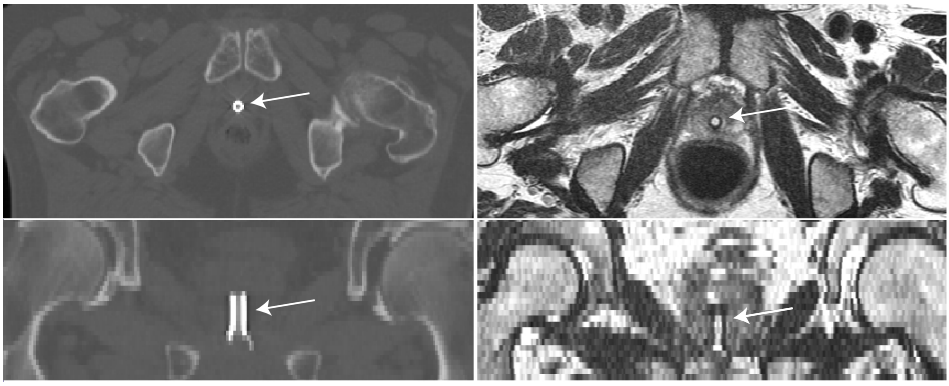

Figure 1.3: An example of the CT image (left) and MR image (right) in the axial (top) and sagittal (bottom) image plane. The white arrow marks the prostate stent in both images.

1.2 Objectives

The motivation of the thesis is to reduce uncertainties related to manual procedures as the procedures are prone to errors and observer variation. These errors are systematic errors and remain constant during treatment and can therefore cause a geometrical miss of the tumor and increased radiation of the surrounding healthy tissues. Medical image analysis has been suggested in a variety of applications to automate the image registration and target delineation, also called image segmentation, to improve the planning of radiotherapy.

The main procedures related to treatment of prostate cancer using IGRT are shown in Fig. 1.4, where the focus of this thesis is MR-CT registration and target delineation in the radiotherapy planning process.

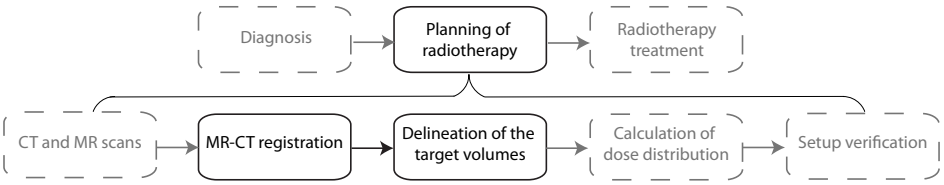

Figure 1.4: The process for prostate cancer treatment using IGRT. First, a diagnosis is made, followed by a planning of radiotherapy, and radiotherapy treatment. The focus of this thesis (solid boxes) is planning of radiotherapy and in particular MR-CT registration and target delineation. Other procedures in the planning process relate to acquisition of MR and CT, calculation of radiation dose distribution, and patient setup in the treatment system.

The objectives of the thesis are to:

- Develop an approach for MR-CT registration of the prostate using a newly developed prostate stent to be able to perform target delineation in MR.
- Compare the MR-CT registration and the currently used manual registration.
- Develop approaches for prostate segmentation in MR to be able to perform automatic prostate segmentation as the CTV.
- Validate the MR-CT registration as well as the prostate segmentation.

2 Image Registration

2.1 Introduction to Image Registration

Image registration is the problem of bringing two or more image data sets into spatial alignment. Thereby, the images can be analyzed in the same coordinate system, which facilitates e.g. monitoring of the progression of the disease or treatment outcome, improved target delineation, creation of statistical models, creation of atlases, or co-registering of different imaging modalities.

This thesis focuses on intra-subject registration of MR and CT to allow target delineation in MR and dose calculations in CT. In image registration, one image data set is called the moving (or source) image and is transformed to align with the fixed (or target) image data set. The registration can have different degrees of freedom associated with the transformation type. Translation registration allows three translations. Rigid registration allows three translations and three rotations. Procrustes registration allows three translations, three rotations, and one global scaling. Affine registration allows three translations, three rotations, three scalings, and three shears. Non-rigid registration allows local elastic deformations of the moving image data set and results therefore in a high-dimensional optimization problem but is often required in inter-subject registration or in registration of organs which can deform over time.

Based on a review by Maintz and Viergever [25] medical image registration approaches can be divided into four categories:

- Non-image-based registration
- Landmark-based registration
- Segmentation-based (also known as surface-based) registration
- Voxel-based registration

These categories will be used in the following to divide the previous studies, which have performed co-registration of MR and CT of the prostate.

Most of the previous work in MR-CT registration of the prostate have focused on rigid registration. This assumes no prostate deformations. However, this assumption is difficult to validate because the shape of the prostate gland is difficult to delineate in the CT image. Instead, the assumption was validated by Carl et al. [24] using two MR scans from the same patient, which were registered using a manual landmark-based registration and very minor difference in shape was observed. Furthermore, Deurloo et al. [26] found no significant variation of GTV during radiotherapy treatments. The variation of GTV was in the order of intraobserver variation and was small compared with the movement of the prostate. Deformations of the prostate are likely to occur when an endorectal coil is used to improve the quality of the MR image [27], where a rigid registration should be used with care and affine or non-rigid registration might be more accurate.

In some of the previous studies the main objective was not the registration itself, but it was used to be able to e.g. compare MR and CT for target delineation as in [13]. In cases where more than one approach have been used e.g. in [28] the categorization is determined by the method, which is believed to bring most weight into the registration. Also, the study in [29] has described and compared two approaches and they will therefore be described separately in the suitable category.

A common objective of the studies is that the registration was used to be able to delineate the CTV in MR and use CT for treatment planning for either external radiotherapy and brachytherapy. Some studies have based the registration of the pelvic bones risking an inaccurate alignment of the prostate caused by the prostate movement, which can occur relative to the pelvic bones. However, the majority of the recent studies have applied a prostate registration using fiducial markers implanted into the prostate gland to obtain prostate alignment in MR and CT.

2.2 Review of MR-CT Registration of the Prostate

2.2.1 Non-image-based Registration

Algan et al. [30] aligned the imaging coordinate systems from the MR and CT scanner by first acquiring the CT images and then the MR images using a patient immobilization device. This approach does not take patient or prostate movement into account but is an alignment of the imaging coordinate systems. As a consequence, Algan et al. [30] also recommended a margin of at least 10 mm added to the CTV.

2.2.2 Landmark-based Registration

A registration based on landmarks is obtained by a selection of corresponding anatomical or geometrical landmarks in both MR and CT. Kagawa et al. [31] registered the bones in MR and CT by selecting three manually defined landmarks in both MR and CT on the pubic symphysis and the sciatic notch. The results showed events of prostate movement due to differences in rectal filling in the time of the CT and MR acquisition, which stresses the importance of a more local registration registration of the prostate. A two-step procedure was applied by Polo et al. [32] in which an automatic step was first performed based on an extraction of common contours in MR and CT, but this is not described in detail in the paper. This was followed by a manual landmark-based registration by selecting three anatomical landmarks on the pelvic bones to improve the registration [32].

Lian et al. [33] used a deformable landmark-based registration because the MR images were acquired using an endorectal coil causing deformation of the prostate between the scans. Four to eight control points were placed on the prostate border in both MR and CT in each slice of the volume. The warping process was carried out using a thin plate spline transformation for each 2D slice. Thereby, the registration was based on an assumption that the prostate border can be extracted from CT. [33] Local prostate features in form of fiducial markers implanted into the prostate gland have been used frequently. Carl et al. [22] defined three landmarks on a removable Ni-Ti prostate stent as a fiducial marker, one at the cranial, middle and caudal end of the stent. Another one or two anatomical landmarks were defined, one anterior and one lateral to the prostate but as close to the prostate surface as possible to limit the influence of the surrounding tissue but in the

same time to constrain rotations about the center axis of the stent. The use of anatomical bone landmarks are not needed when three or more fiducial markers are implanted into the prostate gland. Nevertheless, bone and soft-tissue landmarks were used by Crook et al. [34] to obtain an initial registration, which was refined by a local registration of the prostate based on landmarks defined on the fiducial markers.

Three manually defined landmarks were selected on the center of the gold fiducial markers in the studies by Parker et al. [14] and Huisman et al. [29]. Huisman et al. [29] furthermore validated the observer variation, which was not found to have a statistically significant effect on the registration. Only 42% of the registrations had a precision higher than 2 mm at the prostate border. [29]

2.2.3 Segmentation-based Registration

Segmentation-based registration requires that equivalent surfaces in the two images are segmented. The alignment can then be achieved e.g. by using the iterative closest point, which tries to minimize the distance between two point clouds obtained from the segmentations. A bone segmentation in MR and in CT was used by Rasch et al. [13] and Herk et al. [35]. The segmentation was followed by an automatic tracer to detect the points forming the bone edges and a manual removal of the points caused by artifacts. Based on the edge points, chamfer matching was applied by minimizing the distance between the points within a fixed limit.

Huisman et al. [29] used a manual segmentation of the fiducial markers. It was converted to surface models followed by the iterative closest point approach to minimize the root-mean-square distance between the cloud points from the segmentations in MR and CT. This approach was compared with a manual landmark-based registration and results showed a better performance of the iterative closest point as 86% of the registrations were regarded as clinical acceptable compared with 42% using the landmark-based registration

2.2.4 Voxel-based Registration

Voxel-based registration uses the voxel intensities in the image data sets to find the optimal transformation, which requires that common structures in the two image data sets are visualized. Maes et al. [36] used the similarity measure mutual information to register the pelvic bones in MR and CT as one example of possible applications, which can benefit from the use of a voxel-based registration using mutual information.

Vidakovic et al. [28], McLaughlin et al. [37], and Roberson et al. [38] used voxel-based registration of MR and CT using fiducial markers implanted into the prostate gland to obtain a local registration. The studies had in common that the image resolution and information inside the prostate were found to be too poor to allow for a registration solely based on voxel similarity, which is supported in [14]. Therefore, all three studies have applied a two-step approach. Vidakovic et al. [28] first defined feature lines as a straight line between the center of fiducial markers followed by a determination of the in-plane rotation (in the sagittal and coronal plane) based on the angle between the lines. This rotation was applied to the MR so that the feature lines were parallel. The final registration used normalized mutual information but constrained the rotation to the patient center axis and allowed translation in all three image planes. McLaughlin et al. [37] and Roberson et al. [38] used an initial registration based on manually defined landmarks from the

prostate, the surrounding tissue, or from the fiducial markers. This was followed by a cropping of the volume of interest in MR, where the default cropping contained some of the pelvic bone. In the work by Roberson et al. [38] the volume could be varied by cropping out the rectum, bladder, or the remaining part of the bones depending on the changes between the scans. Roberson et al. [38] found that cropping the volume so that only the prostate was included resulted in reduction of accuracy because the image support was not sufficient to prevent large rotations. The second step relied on voxel information using mutual information as the similarity measure to register the cropped MR data set with the CT data set.

2.3 Validation of Image Registration

Validation of image registration is needed in order to demonstrate performance of the registration. Various validation methods have been suggested to assess the registration quality including visual inspection, comparison with a ground truth registration, contour overlays, and quantitative validation of the robustness and consistency. [39]

Visual inspection provides a qualitative validation of the performance of the registration. Fitzpatrick et al. [40] have investigated the accuracy of a visual validation and found that the human can visually detect target registration errors down to 2 mm for MR-CT registration of brain images [40]. Visual inspection is a crucial part of the validation because a ground truth registration does not exist within prostate registration. In brain registration, West et al. [41] have used skull-implanted markers for brain surgery to establish a ground truth for multimodal rigid registration to which new registration approaches can be compared with. In the absence of a ground truth registration, phantom studies and simulations can be used [25] even though it only resembles the clinical use. In cases where it is possible to extract common structures from the images, contour overlays can be used to validate the registration. This is however not the case for MR-CT registration of the prostate except if the fiducial markers can be extracted with a high accuracy. Otherwise, a segmentation or delineation error will influence the validation of the registration. [39] Quantitative validation of the robustness and consistency of the registration can show the ability for the registration to converge to the same result after changing the registration conditions. It can be validated by adding noise, defining different starting transformations, or to use a registration circuit. The registration circuit can be used if three or more image data sets are available using the approach in Equation 2.1. The first data set (T_1) is registered to the second (T_2), which is then registered to the third (T_3), which is then again registered back to the first image data set. A consistent registration approach will result in an identity transformation (T). [42]

$$T = T_{1\rightarrow 2}T_{2\rightarrow 3}T_{3\rightarrow 1} \tag{2.1}$$

This approach is more suitable for single modal registration than for multi-model registration, as the MR-CT registration does not need to the same as the inverse registration.

2.4 Methods Investigated in this Thesis

Two studies are performed related to image registration of MR and CT. In Paper I, the registration of MR and CT images to obtain an accurate alignment of the prostate is

described. In Paper II, two image registration approaches are compared to investigate the clinical potentials for automating the registration process. Subsection 2.4.1 and 2.4.2 provide in overview of the methodology used in Paper I and Paper II, respectively.

2.4.1 MR-CT Registration using a Ni-Ti Prostate Stent in Image-Guided Radiotherapy of Prostate Cancer

One of the goals of the registration approach presented in this section is that it should be a clinical accepted solution and thus be simple, accurate, and robust. Mutual information is a voxel similarity measure which has been widely used for multi-modal image registration primarily in brain imaging, and is the measure used in this work because it has shown to be accurate and robust [43]. The assumption behind voxel similarity measures relates to comparable intensity values of the region of interest in the two images, where the ratio of the variance of the intensity values in the region of interest should be small. The average variance of this ratio is minimized in the registration and the joint entropy is decreased with increased alignment. [44] Viola and Wells [45] and Collignon et al. [46] simultaneously suggested to use the images mutual information for image registration. The mutual information *I* for the images *A* and *B* is given by:

$$I(A, B) = H(A) - H(B|A) = H(B) - H(A|B), \tag{2.2}$$

where *H(A)* is the entropy of the moving image, *H(B)* is the entropy of the region of the fixed image where the moving image is overlapping, and *H(A|B)* and *H(B|A)* are the conditional entropies of the two images. Maximizing the mutual information *I(A,B)* is obtained by minimizing the joint entropy of the images.

The optimization of the registration using the voxel-based registration approach uses an iterative strategy where an initial estimate of the transformation is refined by calculating the similarity measure between the images. This continues until the algorithm converges to a preset tolerance. A risk related to this approach is that the algorithm is converging towards a local extrema. Therefore, many optimization approaches apply a multiresolution scheme because many of the local extrema are small extrema that can be removed by reducing the image resolution and/or blurring the images before registration. The transformation obtained by registration of the low resolution images or large blurring kernels are used as an initial transformation to the next registration using a higher image resolution or a smaller blurring kernel, and so on.

2.4.1.1 Method Overview

Strategies for maximization of mutual information include choices regarding pre-processing, degrees of freedom in the transformation, interpolation, optimization approach, potential use of multi-resolution strategies, etc. [44] Figure 2.1 gives an overview of the registration approach used in Paper I, which consists of an initial registration of the bones followed by a local registration of a volume tightly surrounding the prostate stent in MR. The two-step procedure makes it possible to achieve a local alignment of the prostate in MR and CT, which is needed due to the prostate movement, which occurs relatively to the pelvic bones. The aim of the first step is to align the pelvic bones, which serves as an initial registration, and enable the use of rotational constraints in the local registration. Rotational constraints are needed because the prostate stent has a shape

of a cylinder, which introduces a risk of unrealistic rotations about the center axis of the stent and therefore most often about the patient center axis. Langen and Jones [18] collected the results from studies investigating the translational movement of the prostate relative to the pelvic bones. The primary axis for translational movement was found in the studies to occur towards the anterior or posterior direction and towards the cranial or caudal direction. The translational movement towards the left or right direction is however limited. The rotation of the prostate has been found to primarily occur in the sagittal plane resulting in translational movement in the cranial-caudal and anterior-posterior direction [47, 48, 49, 50, 51, 52, 53]. These findings are likely to be related to changes in rectum and bladder filling. The rotation about the axial plane is limited which can be explained by the anatomy of the pelvis where the top of the prostate is attached to the bladder and the prostate bottom is attached to the pelvic floor.

The registrations are performed in the registration tool minctracc [54], which uses a trilinear interpolation. Consequently, the image resolution of the two volumes does not need to be the same and a sub-voxel optimum of registration can be found. In both the initial registration and in the local registration, a simplex optimization method is used. The simplex optimizer does not require calculation of derivatives, it converges to the optimal registration fast, and it considers all degrees of freedom simultaneously. [44] In minctracc the simplex volume is measured in millimeters of translation and degrees of rotations. The better the initial registration is believed to be, the lower the simplex search radius should be [55]. Therefore, the simplex is reduced for each registration level and only small adjustments are possible in the last step of the registration.

2.4.1.2 Initial Registration

The initial registration uses a multi-resolution strategy with increased image resolution of 8, 4, 2, and 1 mm. The advantage of a multi-resolution strategy is two-fold. First, it reduces the computational demand of the registration and reduces the risk for that the registration is trapped in a non-global optimum [44].

The difference in the center of gravity of the MR and of the CT is calculated, which serves as a starting translation of the first iteration of the initial registration. Thereafter, an iterative registration is performed using the multi-resolution scheme, in which the simplex radius is also decreased.

2.4.1.3 Local Registration

A volume closely surrounding the prostate stent is defined by manually cropping the MR images. Alternatively, a manual delineation of the prostate as the CTV could have been used as a mask in the registration. Rotational constraints are defined in minctracc by not allowing rotations about the patient center axis due to the risk for unrealistic rotations about the stent. Instead of decreasing the image resolution, Gaussian blurring is used to reduce the risk for that the registration is trapped in a non-global optimum. The blurring kernels and simplex radius are iteratively decreased.

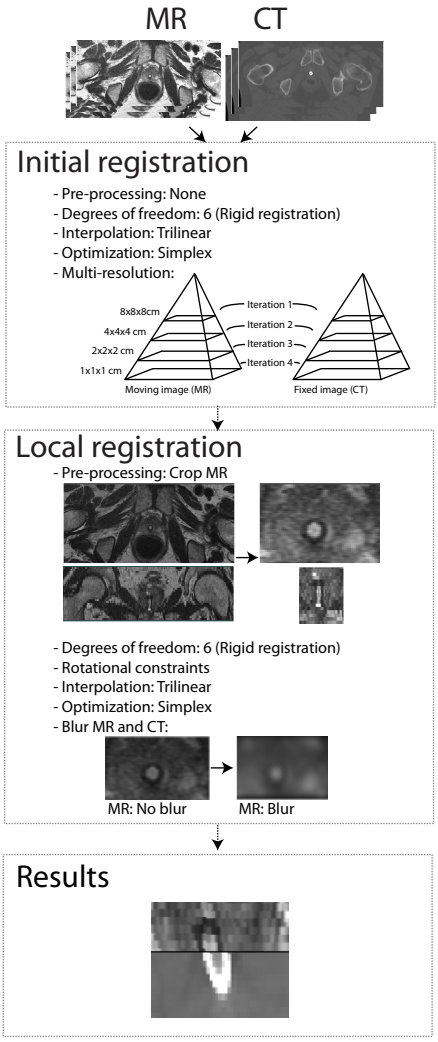

Figure 2.1: The two-step MR-CT registration of the prostate.

2.4.2 Comparison of Manual and Automatic MR-CT Image Registration for Image-Guided Radiotherapy of Prostate Cancer

Two registration studies are compared. The first registration approach is a manual registration based on manually defined landmarks as described by Carl et al. in [22]. The second registration approach is the automatic two-step approach described in the previous section and Paper I.

A manual delineation of the prostate as the CTV in MR is available for all image data sets. The CTV is registered with both the manual landmark-based registration and with the automatic voxel property-based registration, see Figure 2.2. Therefore, similarity

measures in form of sensitivity and Dice similarity coefficient (DSC) [56] between the volumes after registration using each of the approaches can be determined.

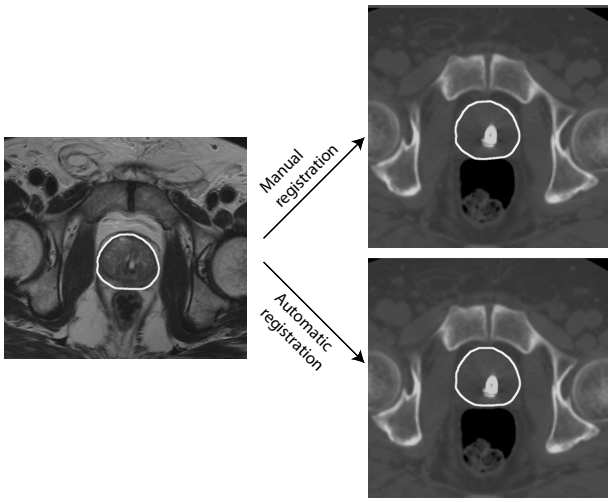

Figure 2.2: The manual delineated CTV in MR is registered with both the manual registration approach and with the automatic registration approach, which enables that translational and rotational differences as well as overlap measures can be computed.

Figure 2.3 illustrates the CTV registered with the manual (green) and automatic (white) registration approach with corresponding DSC values for the three examples. Random selected points within the CTV is transformed with each registration approach to be able to calculate a translational and rotational difference of the prostate between the two registration approaches. Furthermore, the clinical potential of the automatic registration approach is discussed based on the fact that the manual registration is already used today at Aalborg University Hospital and results have indicated reduced longterm toxicities compared with the standard treatment using CT for target delineation [57].

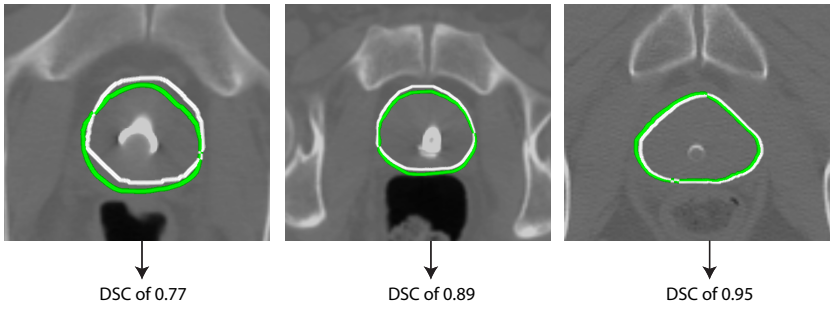

Figure 2.3: The axial view of the overlap of the CTV superimposed on the CT images from the manual registration (green) and the automatic registration (white). The corresponding DSC is shown for each example.

Figure 2.4 shows the correspondence between the prostate, the bladder, and the rectum superimposed on the CT image. The volumes are all manual delineated on the original MR data set and then transformed to align the CT data set with the manual approach and the automatic approach.

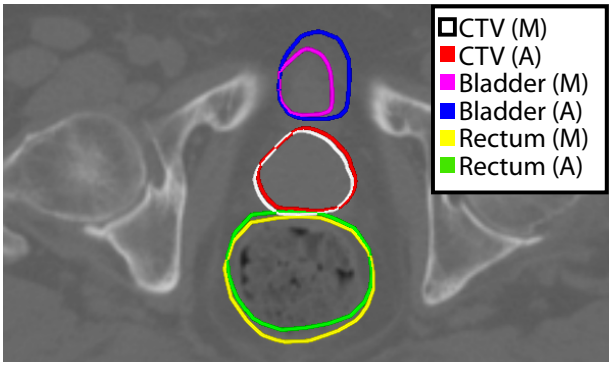

Figure 2.4: The CTV and the surrounding critical organs, bladder and rectum, superimposed on the CT image. The volumes are transformed with the automatic approach (A) and the manual approach (M).

3 Image Segmentation

3.1 Introduction to Image Segmentation

Image segmentation is the problem of partitioning an image into two or more separated regions, the foreground or region(s) of interest and the background. This thesis focuses on a segmentation of the prostate in MR as the CTV used for planning radiotherapy of prostate cancer.

Based on a review by Pham et al. [58] segmentation methods for medical images can be divided into the following categories:

- Thresholding
- Region growing
- Classifiers (supervised segmentation)
- Clustering (unsupervised segmentation)
- Markov random field models
- Artificial neural networks
- Deformable models or active contours
- Atlas-based segmentation
- Other approaches (e.g. edge detection and watershed)

In addition, statistical models are popular in medical image segmentation as a-priori information about the statistical characteristics of the object is used in the segmentation [59].

These categories will be used to divide the previous studies, which have performed prostate segmentation in MR. Not all methods have been applied for prostate segmentation and the following will only focus on applied methods.

The clinical practice for defining the CTV or prostate delineation is today widely performed using a manual contouring of the prostate slice-by-slice using either the axial, coronal, or sagittal view or a combination of the views. However, the manual work is a labor-intensive and time-consuming task and is prone to interobserver and intraobserver variation [16, 17]. To reduce these uncertainties several authors have described semi- or automatic methods for prostate segmentation in MR in either 2D or 3D.

Prostate segmentation in MR images is a challenging task because the intensity distribution inside the prostate gland is characterized by voxel inhomogeneity. Therefore, an accurate prostate segmentation cannot rely on intensity information alone as in e.g. thresholding and region growing. Few authors have based their methods on intensity information yet incorporated additional knowledge about the general prostate shape in the

segmentation. Most studies have used either atlas-based methods, deformable methods, or statistical models. The categorization of the applied methods is of course not definitive as a combination of methods can be beneficial for the performance. The categorization is in these cases determined by the method, which is believed to bring most weight into the segmentation. The different approaches will be described briefly based on the categorization above, however, all methods based on voxel information are described under the category voxel-based. Only studies working with prostate segmentation in MR are described. For an overview for the segmentation in ultrasound and CT, see e.g. the review by Ghose et al. [60]. In addition to the following description of segmentation approaches, the Prostate MR Image Segmentation (PROMISE12) challenge was held together with MICCAI2012, where participants submitted their results using the same data sets and the studies can therefore be directly compared. Litjens et al. [61] collected the different methodologies and results.

3.2 Review of Prostate Segmentation in MR

3.2.1 Voxel-based

Voxel-based methods use intensity values to separate the image into regions e.g. using edge detection, one or more threshold values, or by assuming connectivity of similar pixels in a region. [58] Flores-Tapia et al. [62] selected four points manually at the top, left, right, and the lower part of the prostate. A multiscale wavelet transform was used to detect edges, which was followed by a set of spatial rules about the prostate shape. Ellipse contours in the superior end and inferior end of the prostate and a cardioid contour in the middle of the prostate were assumed. Zwiggelaar et al. [63] used a user defined prostate center and the image ridges were detected using a polar transform in 2D, which was followed by non-maximum suppression. The prostate border was defined as the longest curvilinear structures.

3.2.2 Atlas-based

Atlas-based segmentation turns the segmentation problem into a registration problem. An atlas is created using a training set with manual delineations of the object of interest. The atlas represents the probability for that a given voxel belongs to the object of interest. The atlas is then registered to the target image. [58] Probabilistic atlas segmentation has been used by Ghose et al. [64] and by Martin et al. [65], where the probabilistic atlas was registered with the target image. Further processing was used to improve the segmentation quality. Ghose et al. [64] used graph cuts for energy minimization of the posterior probabilities for a voxel to be a part of the prostate, which was obtained by the atlas-based segmentation and a random forest classification. Martin et al. [65] used user-defined points on the prostate border to improve the registration of the atlas with the target image and to incorporate shape constraints in the segmentation.

The majority of the previous studies have used multi-atlas segmentation as it generally is considered to be more accurate than a single atlas or a probabilistic atlas [66]. Klein et al. [67] used an automatic multi-atlas segmentation and majority voting fusion. The segmentation was based on a pairwise registration followed by atlas selection based on image similarity using normalized mutual information between the target image data

set and each atlas image data set. Dowling et al. [68] added a preprocessing step to the approach suggested in [67] using the same data set and performed a comparison of multi-atlas segmentation and a probabilistic atlas in which the multi-atlas segmentation had the highest accuracy. Langerak et al. [69] also used multi-atlas-based segmentation with a focus of improving the atlas fusion strategy. A combination of atlas selection and performance estimation strategies was used in an iterative procedure called Selective and Iterative Method for Performance Level Estimation. This work was continued in [70] where atlases were clustered so that each cluster only contained atlases which registered well to each other. The decision of the most suitable cluster was based on registration of one atlas image from each cluster to the target image. The cluster with the atlas image, which has the highest estimated performance, was chosen and all atlas images in this cluster were then registered with the target image using multi-atlas registration.

3.2.3 Deformable Models

Deformable models segment the boundary of the region of interest based on closed parametric curves or surfaces placed near the desired boundary. The curve or surface will then deform under the influence of internal and external forces. [58] Deformable models have been used by Martin et al. [71], Chandra et al. [72], Pasquier et al. [73], and Makni et al. [74] to deform an atlas or shape model to the target image.

Martin et al. [71] and Chandra et al. [72] used non-rigid atlas registration to obtain an initial atlas-based segmentation using a probabilistic atlas and multi-atlas-based approach, respectively. This segmentation was then used to initialize the deformable model, which was regularized using a statistical shape model, image features and spatial constraints to ensure only anatomical possible deformations. Chandra et al. [72] first found the most similar atlas images based on normalized mutual information, which were then used to create the atlas.

Pasquier et al. [73] and Makni et al. [74] used a landmark-based active shape model which was automatically deformed using deformable models to the prostate. Makni et al. [74] added an extra step in form of a Bayesian classification framework to the method.

3.2.4 Statistical Models

Statistical models consist of shape models and active appearance models (AAM) which are both based on training data. Shape models represent the object of interest statistically by analyzing the variation across the training set, hereafter the model is used to segment the target image. AAM is an extension of the shape model in which the texture e.g. the intensities of the object, is statistical described and included in the shape model. [59] Chowdhury et al. [75] used both MR and CT in the segmentation as an extension of the work in [76]. A shape model was obtained after registration of MR and CT and training samples of prostate in both CT and MRI were used so that the shape variations in MR and CT were linked in the two imaging modalities. Tsai et al. [77] used a level-set representation of the object shape. The work was motivated by a wish to eliminate the need for manual landmark selection and point by point correspondence in the shape model. The shape model was obtained by a principal component analysis (PCA) of a collection of signed distance representations of the shapes of the training images. Segmentation of the prostate was used to show a potential application. A level-set representation of the

prostate shape was also used by Toth and Madabhushi [78] in an AAM segmentation. Texture information contained image derived features such as the image intensities and gradient information. AAM was also used by Ghose et al. [79] but here manually defined points in the training data sets were used to represent the prostate shape, which was propagated by the approximation coefficients of Haar wavelet transform in 2D.

3.3 Validation of Image Segmentation

Validation is needed in order to demonstrate segmentation performance and to compare the results with other studies. Various validation methods have been suggested to assess the segmentation quality, where visual inspection and comparison with a ground truth segmentation using different similarity metrics are the two most frequently used methods. Visual inspection is an important qualitative validation of the accuracy of the segmentation. A ground truth segmentation is often defined as a manual segmentation of the same object to allow for a quantitative validation. However, the manual segmentation is prone to inter-observer variation [16, 17] and is therefore only the best available candidate for a ground truth segmentation. Therefore, several studies e.g. [67, 68] have two or more observers to perform the same segmentation to determine the interobserver agreement to which the proposed similarity metrics can be compared with. Often used similarity metrics within prostate segmentation are DSC, mean surface distance (MSD), and hausdorff distance.

A comparison of the results from different studies should be accepted with care because different imaging protocols have been used. For example, Toth and Madabhushi [78] used MR images acquired using an endorectal coil, which makes the prostate boundary easier to detect. The same data set should be used to directly compare the results, e.g. the data set from the PROMISE12 challenge [61].

3.4 Methods Investigated in this Thesis

In Paper III, the development of a prostate segmentation in MR using an AAM with a level-set representation of the shape is described. In Paper IV, the development of a prostate segmentation in MR combining shape obtained from atlas registration and intensity information in a graph cut framework is described. Further, Subsection 3.4.1 and 3.4.2 provide an overview of the methodology used in Paper III and Paper IV, respectively.

3.4.1 Active Appearance Modeling using Level-set Representation of the Prostate Shape

Statistical models can be used to provide knowledge about the object variability between subjects, which can be derived in a training phase. The idea behind statistical models is that it is possible to learn plausible variations of the objects prior to segmentation. An often used statistical model for image segmentation is active shape models suggested by Cootes et al. [80]. The training of the model is used to determine the possible deformations of the model to the target image. An extension of the active shape model is the AAM [81, 82] in which a statistical model of the object shape and the appearance of the texture of the object can be combined to add additional knowledge into the segmentation

model. The texture model is used to model the image intensities or other features. The traditional AAM is built in a training phase using anatomical landmarks placed on the object border.

The assumption behind AAM is that changes in the shape and the texture of a given object are correlated. The AAM presented here is a PCA-based statistical model where a shape model and a texture model are combined, described with the same set of parameters.

3.4.1.1 Method Overview

The overall approach for the use of an AAM can be divided into five main procedures:

- Alignment of training images
- Modeling shape variation
- Modeling texture variation
- Combining the shape and texture models in the AAM
- Fitting the AAM to the target image

The segmentation approach applied here combines texture and shape information in an AAM using a level-set representation of the prostate shape. The methodology used is suggested by HU and Collins [83] and Stephansen [84]. An overview of the creation of the AAM and the segmentation of the target image is shown in Figure 3.1

3.4.1.2 Alignment of the training images

Prior to the creation of the shape and texture model, an alignment of the training images is performed. In this work, a common reference image is chosen to which the remaining training images are registered to using the Procrustes registration and the voxel similarity measure mutual information in the registration tool minctracc [54].

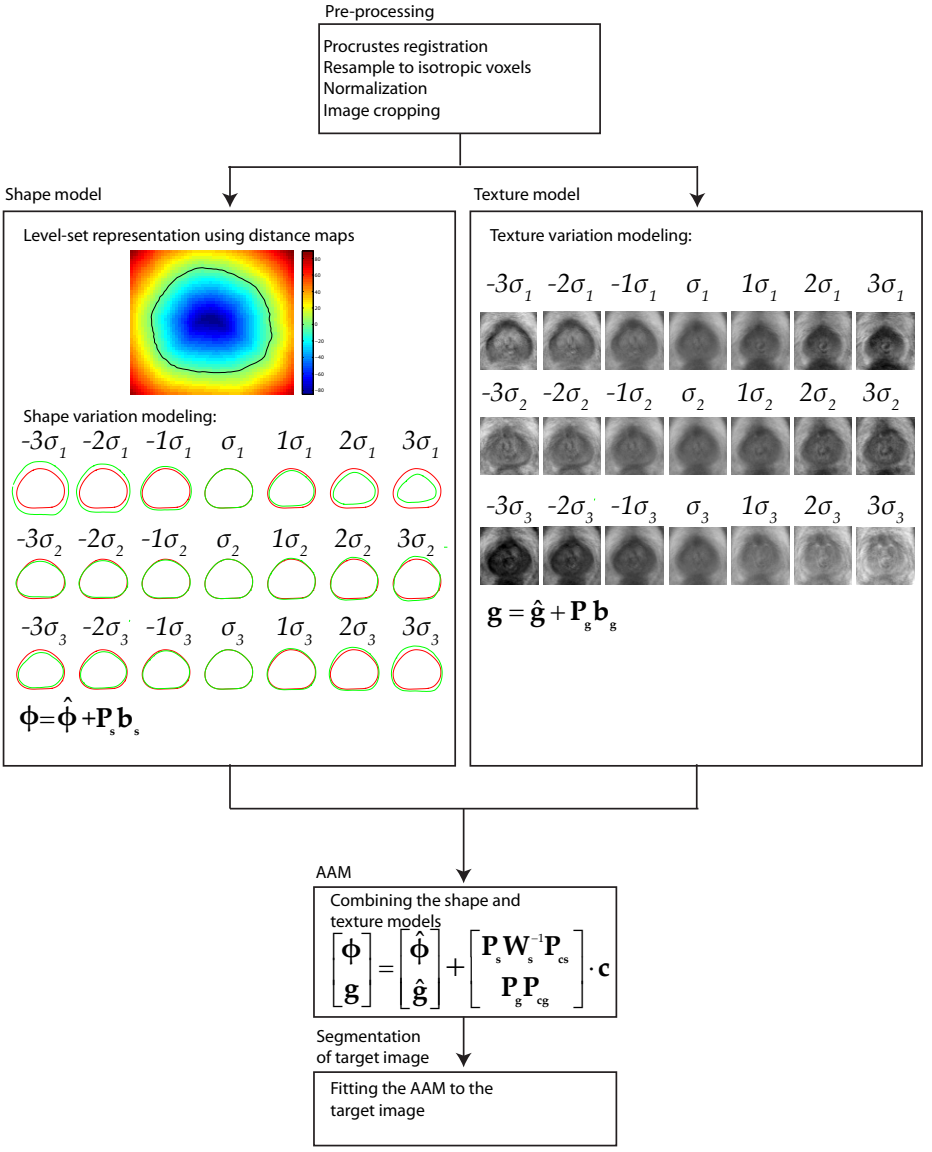

Figure 3.1: Overview of the segmentation approach. A level-set representation of the shape is used to create the shape model of the shape variation. The texture model consists of a modeling of the image texture and is combined with the shape model to define an AAM. The AAM is then fitted to the target image to segment the target image.

3.4.1.3 Modeling Shape Variation

The traditional AAM requires a manual selection of landmarks at the object border to create a shape model based on the mean and variation of the landmark positions [81]. It is a time-consuming task as well as it is prone to errors because the user needs to be able to place the landmarks in the same position in all training images to prevent problems with correspondence [85]. An alternative approach for selection of landmarks is based on automatic landmark selection. However, this is also prone to errors [86]. Consequently, a more recent approach based on a level-set representation is applied to eliminate the need for landmark selection. Signed distance functions are used to represent the prostate shape [87, 86]. The shortest distance from each image point to the prostate border forms the distance map. The image points inside the object are assigned with negative values and image points outside the object are assigned with positive values. The image points forming the object border are assigned with the value zero. [77] A shape model based on signed distance maps still requires correspondence between the training images, which is achieved in the alignment of the training images.

The shape model is a linear statistical model and is based on a PCA, which models the possible modes of variation of the mean shape. The shape model consists of mean shape, the possible modes of variations (eigenvectors), and the range of the modes (eigenvalues). The shape can be modeled in a linear combination [83]:

$$\boldsymbol{\phi} = \widehat{\boldsymbol{\phi}} + \mathbf{P}_s \mathbf{b}_s, \tag{3.1}$$

where $\widehat{\boldsymbol{\phi}}$ is the mean shape, $\mathbf{P}_s$ is a set of eigenvectors describing the principal modes of shape variation, and $\mathbf{b}_s$ is the weight coefficient vector. Adjusting $\mathbf{b}_s$ will result in various shapes or signed distance functions. Spurious variations and noise are removed from the training by removing the eigenvectors with the smallest eigenvalues, here the threshold is set to 0.98% suggested by Cootes et al. [85].

3.4.1.4 Texture Model

The texture model is a linear model consisting of gray image intensities. As for the shape model, the texture model is constructed using PCA. Therefore, the texture is also modeled in a linear combination [83]:

$$\mathbf{g} = \widehat{\mathbf{g}} + \mathbf{P}_g \mathbf{b}_g, \tag{3.2}$$

where $\widehat{\mathbf{g}}$ is the mean intensity, $\mathbf{P}_g$ is a set of eigenvectors describing the principal modes of texture variation, and $\mathbf{b}_g$ is the weight coefficient vector describing the texture parameters. Adjusting $\mathbf{b}_g$ will result in various textures.

3.4.1.5 Active Appearance Model

The aim of the AAM is to describe both the shape and texture of the training data. The two models are combined and by varying the appearance parameters $\mathbf{c}$ new images and shapes can be synthesized.

$$\begin{bmatrix} \boldsymbol{\phi} \\ \mathbf{g} \end{bmatrix} = \begin{bmatrix} \widehat{\boldsymbol{\phi}} \\ \widehat{\mathbf{g}} \end{bmatrix} + \begin{bmatrix} \mathbf{P}_s \mathbf{W}_s^{-1} \mathbf{P}_{cs} \\ \mathbf{P}_g \mathbf{P}_{cg} \end{bmatrix} \cdot \mathbf{c},$$

where $\mathbf{P}_{cs}$ and $\mathbf{P}_{cg}$ represent the shape and texture part of the principal modes of appearance variation. The appearance parameters $\mathbf{c}$ values are constrained to the interval of ± 3 standard deviations as in [82]. $\mathbf{W}_s$ is a weight matrix to account for potential differences between the shape and texture units. The weight matrix is determined by the ratio of the image intensity variation to the shape variation.

3.4.1.6 Fitting the AAM to the Target Image

The last step in the segmentation process using AAM is to fit the AAM to the target image also known as segmentation of the target image. The fitting process seeks to find the AAM model parameters which generate a model image closely corresponding to the target image. These model parameters are learned prior to segmentation, so that only plausible variations of the prostate shape and texture are tried. To ensure that all possible shapes are generated each of the AAM parameters are constrained to be within ± 3 standard deviations. [85]

3.4.2 Atlas Registration and Intensity Modeling

3.4.2.1 Atlas-based Segmentation

Atlas-based segmentation methods convert the segmentation problem into a registration problem. Atlas-based segmentation has been widely used for segmentation problems and is based on the atlas image consisting of an intensity image and a corresponding labelled image. The different registration methods mentioned in Section 2.1 can all be used to create an atlas. However, the voxel-based approaches are recommended because they do not require prior segmentation or user-interaction e.g. by selecting landmarks. Moreover, most atlases are based on affine and/or non-rigid registration because the atlases are based on inter-subject registrations and therefore need to be able to include the anatomical variations between subjects.

Three types of atlases exist, single atlas, probabilistic atlas, and multi-atlas. The single atlas is also called topological atlas or deterministic atlas and is based on a single subject. The atlas is often selected so that it represents the average shape of the object of interest. As a result, the atlas does not represent the diversity of the anatomy. To better represent the diversity, probabilistic atlases have been used in brain segmentation [54] and few studies have focused on the creation of atlas of the prostate in [88, 89]. The probabilistic atlas consists of a smoothed intensity image and a corresponding probability map representing the average anatomical variation. The probabilistic atlas can then be registered to the target image. Multi-atlas is subject-specific and is believed to be more accurate compared with the other atlas-based approaches [90]. The higher accuracy of the probabilistic atlas and the multi-atlas compared with the single atlas can be explained by registration errors as each propagated segmentation might classify a voxel in the target incorrect. However, if these errors are random, which is likely to be true if the atlas is created by data sets from different patients, the registration errors will be corrected using several data sets in the atlas. The creation of the multi-atlas is based on a pairwise registration of the atlases to the target image. Thereafter, label fusion is performed with all registered atlases to obtain a final segmentation of the target image. The most frequently used method for label fusion is the majority voting where the label that the majority of all registered atlases predict to be the target is used as the final segmentation. A drawback is

that is a computationally heavy task and time-consuming to create the atlas as it requires pairwise registrations to the target image. [66]

In this work the registration tool Elastix [91] is used for all registrations and a multi-atlas segmentation is used because of the high accuracy. The first step is a three-step multi-resolution registration approach using the voxel similarity measure normalized mutual information. The registrations are then used to create a subject-specific atlas.

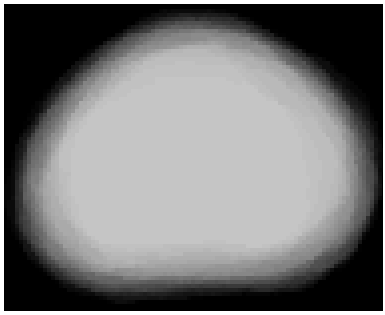

Figure 3.2: An example of the subject-specific probability map. The atlas-based segmentation is obtained by majority voting, where a voxel with a probability higher than a preset threshold is assigned as the atlas.

In this thesis multi-atlas-based segmentation using majority voting label fusion is used as one candidate for prostate segmentation. The final segmentation is obtained by thresholding the probability map so that the segmentation is determined by majority of the labels.

The accuracy of the atlas-based segmentation can be improved using more atlases but that will also make the segmentation of the target image more computational heavy. Therefore, a potential improvement of the atlas-based segmentation in form of atlas selection is suggested. [92]

3.4.2.2 Atlas selection

Atlas selection is a potential extension to atlas-based segmentation to improve the accuracy instead of increasing the number of atlases. Different atlas selection strategies have been used e.g. based on the similarity between the atlas images and the target image [67, 72]. Another approach is to select a fixed number of atlases and then choose the atlases with the highest image similarity with the target image or to use derived similarity from the subjects meta-information e.g. age or cancer stage [92] or to cluster the must similar atlases [70]. The atlas selection used in this thesis is based on the image similarity normalized mutual information between the target image and the atlas images. The atlas images within a threshold of 0.98 of the maximum normalized mutual information between the atlas and the target image are selected. If less than 10 atlases meet this criteria, the 10 atlases with the highest similarity with the target image are selected to maintain a variability in the atlas population.

3.4.2.3 Combination of Intensity and Shape Information

Van der Linj et al. [93] have suggested to combine intensity information and atlas-based segmentation to add additional knowledge into the atlas-based segmentation for hippocampus segmentation. Thereby, the shape prior is supported by intensity information in cases when the segmentation based only on the registrations is insufficient for an accurate segmentation. This idea was applied by Fortunati et al. [94] for head and neck segmentation in CT. The methodology described in this section is based on Kumar and Hebert [95], van der Lijn et al. [93], and Fortunati et al. [94]. Figure 3.3 gives an overview of the method.

Applying Bayes' rule to the segmentation problem, the problem can be divided into shape and image intensity parts based on prior knowledge. The optimal segmentation given the combination of the shape and intensity information is found at the maximal posterior probability $p(\mathbf{f}|\mathbf{i})$, which is defined as the maximum a posteriori probability (MAP):

$$\hat{\mathbf{f}} = \arg\max_{\mathbf{f}} p(\mathbf{f}|\mathbf{i}) \tag{3.3}$$

where $\mathbf{f}$ is the total label configuration and $\mathbf{i}$ is the observed intensity for each voxel in the image. $p(\mathbf{f})$ is the prior probability which does not take any information about $\mathbf{i}$ into account. $p(\mathbf{i}|\mathbf{f})$ is the likelihood that $\mathbf{f}$ will occur if $\mathbf{i}$ is true, or the likelihood for a label to occur if the voxel according to the intensity model belongs to the prostate. $p(\mathbf{i})$ is the marginal likelihood which acts as a normalizing constant.

Prior knowledge and observations of the data sets are used to find the optimal solution. It can be computed by minimizing a posterior energy as in [93] where $p(\mathbf{f}|\mathbf{i})$ is expressed as an energy minimization problem, which consists of an intensity energy term and an a prior energy term. The prior energy can thereafter be approximated by a Markov Random Field.

In this thesis another approach for approximating $p(\mathbf{f}|\mathbf{i})$ is used as in [94]. The approach uses Discriminative Random Fields [95] assuming that the image intensities only depend on the neighboring voxels.

A discriminative random field is given by an association potential and an interaction potential. The association potential combines the shape (spatial prior) and intensity information (intensity model) for each voxel ignoring the effects on all other voxels. Therefore, the interaction potential is added using a neighbor model because a piecewise smooth segmentation is wanted. The association potential and interaction potential are then combined in a graph cut segmentation. The maximum of the MAP is found using graph cuts finding the minimum cut and therefore the optimal segmentation.

Spatial Prior The spatial prior is determined using subject-specific multi-atlases as previously described. A weight parameter λ_2 is added to the spatial prior, which works as a balance term between the spatial prior and the intensity model.

Intensity Model The probability function for the voxel intensities is estimated from the atlases by taking samples from the background and from the foreground. This results in a histogram of both the foreground and the background see Figure 3.4 using a Parzen window approach with a Gaussian kernel. The intensity model is added to correct potential registration errors and will typically have more weight if the histograms are separated further from each other.

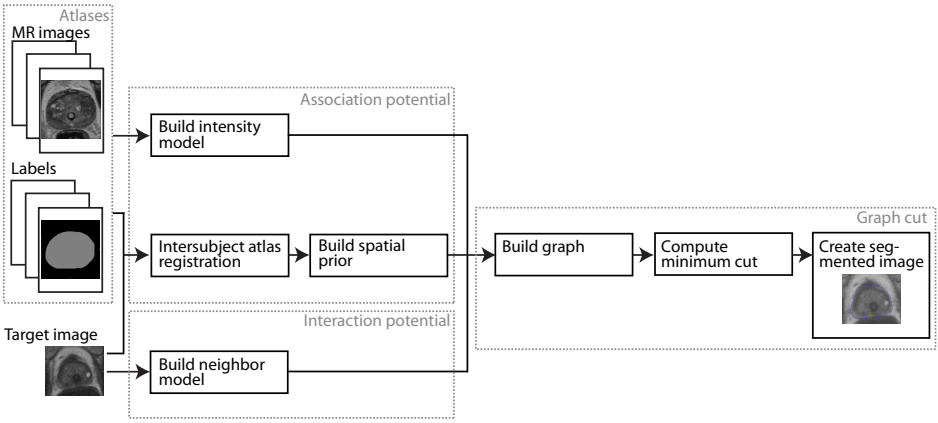

Figure 3.3: Overview of the segmentation approach. Atlas images consisting of MR images and corresponding labeled images are used to create the association potential consisting of both the intensity model and the spatial prior model. Based on the intensities of the target image, the interaction potential is determined to provide a smooth segmentation of the prostate. The potentials are then combined in a graph cut segmentation.

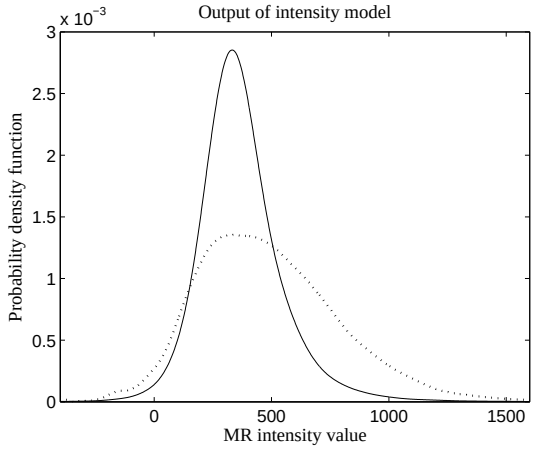

Figure 3.4: The probability function of the foreground (solid line) and the background (dotted line).

Interaction Potential The interaction potential is an intensity dependent smoothing function to obtain smooth segmentations. This is needed because each voxel is handled individually in the association potential. Figure 3.5 shows the prostate segmentation without interaction (left) and with the interaction potential (right), which results in a more smooth segmentation.

Figure 3.5: Comparison of the segmentation without the used on the interaction potential (left) and with the interaction potential (right).

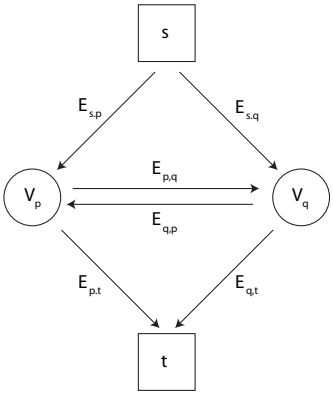

Figure 3.6: A 1x2 voxel image showing the sink, terminal, nodes, and the weighted edges.

3.4.2.4 Graph cuts

Graph cuts have previously been applied for image segmentation to minimize energy functions [96]. A graph cut algorithm for optimization is here used to globally minimize the energy function derived from the MAP equation (Equation 3.3). Figure 3.6 shows a graph used to find the optimal segmentation of a 1x2 voxel image. The weighted graph *G=(E,V)* consists of a set of nodes (*V*), which here correspond to voxels, a set of weighted edges (*E*) that connects the nodes, and two terminal nodes called the source (*s*) and the sink (*t*). There are two types of edges, t-links and n-links. Edges that connect a node to one of the terminals are called t-links (determined by the association potential) and edges that connect two nodes are called n-links (determined by the interaction potential). An s-t cut will divide the nodes into two disjoint subsets *S* and *T* in a way so that the source *s* is in subset *S* and the sink *t* is in subset *T*. If the terminal *t* and the terminal *s* are considered as the foreground class label and the background class label, respectively, then partitioning the nodes are the same as a labeling of the voxels. Finding the minimum energy corresponds to finding the minimum cut. The minimum cut is here computed using the maxflow/min cut algorithm suggested by Boykov and Kolmogorov [97]. Each voxel corresponds to a node in the graph and the graphs minimum cut results in a segmentation of the target.

4 Paper Contributions

In this thesis approaches to automate the MR-CT registration using the Ni-Ti prostate stent and to automate the prostate delineation in MR are developed. This has resulted in four papers which all contribute to the target delineation and image registration processes.

Paper I - MR-CT Registration using a Ni-Ti Prostate Stent in Image-Guided Radiotherapy of Prostate Cancer

The paper presents a local constrained registration of MR and CT based on a newly developed removable Ni-Ti prostate stent as the fiducial marker. The registration uses the voxel similarity measure mutual information in a two-step approach in which the pelvic bones are used to establish an initial registration for the local registration. This is followed by a local registration in which the MR data set is cropped so it contains a region of interest that tightly surround the stent. This is done to avoid that the registration is influenced by pelvic bones and other neighboring structures to the prostate. In order to reduce aperture problems related to rotations around the center axes of the stent, rotational constraints are specified for the mutual information optimization procedure.

Paper II - Comparison of Manual and Automatic MR-CT Image Registration for Image-Guided Radiotherapy of Prostate Cancer

The paper presents a quantitative and qualitative comparison of the automatic registration approach presented in Paper I and a manual landmark-based registration approach. Several comparisons are presented including a computation of difference in rotations and translations of the prostate volume, visual inspection, and a computation of the CTV overlap after transformation of each registration approach. Furthermore, the potential for introducing the automatic registration approach into clinical practice is theoretically investigated by extending the CTV with the registration error of the automatic registration and thereafter calculating the CTV overlap.

Paper III - The use of an Active Appearance Model for Automated Prostate Segmentation in Magnetic Resonance

The paper presents a method for automatic prostate segmentation in T_2-weighted MR images using an AAM incorporating shape and texture information. The model is based on a PCA of shape and texture features with a level-set representation of the prostate shape instead of the selection of landmarks in the traditional AAM. To achieve a better fit of the model to the target image, prior knowledge to predict how to correct the model and pose parameters is incorporated. The segmentation is performed as an iterative algorithm to minimize the squared difference between the target and the model image. The segmentation is compared with manual delineations of the prostate used as the CTV in the planning of radiotherapy.

Paper IV - The use of Atlas Registration and Graph Cuts for Prostate Segmentation in Magnetic Resonance Images

The paper presents a method for automatic prostate segmentation in T_2-weighted MR images combining a spatial prior and intensity information. The spatial prior is based on an inter-subject atlas registration resulting in a subject-specific atlas and the intensity information is based on a statistical intensity model learned from the training data. The shape

and intensity information is combined in a graph cut framework. The method is compared with multi-atlas-based segmentation using majority voting label fusion and with an extension in form of atlas selection.

5 Discussion and Conclusions

5.1 Discussion

This thesis contributes to the field of planning IGRT of prostate cancer to reduce uncertainties related to manual procedures. The two processes related to spatial alignment of the imaging modalities MR and CT and the manual target delineation in MR were investigated. The objective of the PhD studies is to automate these procedures to reduce inter-observer variations related to the manual registration and the manual target delineation. The first step to achieve this goal was a presentation of a widely used method for image registration using the similarity measure mutual information to obtain an automatic and local MR-CT registration. Furthermore, the registrations were compared with the current manual landmark-based registration. The second step to achieve more automation was presented in the second part of the thesis, which focused on automatic target delineation in MR. For this purpose the prostate was segmented as the CTV using two approaches which combine shape and intensity information to improve the accuracy of the segmentation. The first approach presented was an AAM using a level-set representation of the shape. The second approach presented combines a spatial prior and intensity information in a graph cut framework. All investigated approaches were qualitatively as well as quantitatively validated.

5.1.1 MR-CT Registration

The MR-CT registration is an alignment of the two image data sets used for the planning of radiotherapy of prostate cancer. The movement of the prostate relative to the pelvic bones remains a source of errors. The movements can occur during treatment sessions (intrafraction), between treatment sessions (interfraction), and between the scans. The uncertainty of the position of the prostate limits the optimization of more conformal radiotherapy and limits the possible dose escalation. Previous studies have performed registration of MR and CT using fiducial markers as the common structures in MR and CT to obtain a local alignment of the prostate and account for prostate movement between scans. Paper I addressed the challenge of the prostate movement using a fiducial marker for obtaining a local registration of the prostate in MR and CT.

The fiducial marker used in the registration studies presented in this thesis is a removable Ni-Ti prostate stent used at Aalborg University Hospital for registration of MR and CT and for patient setup in the treatment system [24, 22]. The disadvantage of the stent is the shape of a cylinder, which makes anatomical rotations about the center axis of the stent possible. Therefore, an automatic registration requires rotational constraints or inclusion of part of the pelvic bones. This is not needed for other fiducial markers e.g. gold markers because typically three or more are inserted into the prostate gland. However, the prostate stent has several advantages over gold markers including the size of the stent, which makes it clearly visible in both MR and CT. The gold markers can, on the contrary, be difficult to automatically locate in MR because they appear as a signal void, which

was seen in [28, 37, 38, 14]. Furthermore, the low migration risk of the stent makes it possible to regard an accurate alignment of the prostate stent as an accurate alignment of the prostate in MR and CT.

A general issue in image registration is the lack of ground truth registration, which a proposed registration can be compared with. Therefore, a phantom study and visual inspection were used to validate the accuracy, whereas the consistency was validated by applying displacements to the first step of the registration.

The lack of a ground truth registration also complicates a comparison of registration approaches. A comparison of the developed automatic registration approach using mutual information from Paper I and the currently used landmark-based registration was addressed in Paper II. Both approaches use a rigid registration because the prostate is not assumed to deform between the scans. The assumption is based on the image acquisition, where no endorectal coil was used to improve the prostate visualization in MR. The drawback of the endorectal coil is that it can deform the prostate [27]. Because both approaches use a rigid registration, a direct comparison between the registration approaches is possible. Also, the overlap between the manual delineation after registration was calculated. The landmark-based registration is manual and is therefore prone to interobserver variation and it was therefore not possible to determine the most accurate registration approach. However, the manual registration is still accepted to be the closest to a possible ground truth and the clinical experience makes it the one that potentially should be replaced. The landmark-based registration has been used at Aalborg University Hospital for several years to enable MR CTV delineation followed by the radiation dose calculations on CT. This procedure has shown to decrease the CTV and results indicate that the long-term toxicities are reduced compared with the standard CT CTV delineation [57].

Validation showed that the automatic registration approach produced accurate alignment of the prostate stent in MR and CT, which is required to be implemented into clinical practice. Furthermore, the automatic registration has the advantage over the manual registration that it limits the interobserver variation.

5.1.2 Prostate Segmentation in MR

An accurate delineation of the CTV can reduce the PTV because the uncertainties in the delineation process are reduced, which is required to permit dose escalation and improved radiotherapy treatment of prostate cancer. MR is increasingly used for segmentation of the prostate as the CTV because the soft-tissue visualization is better than on CT. The majority of previous studies has performed prostate segmentation in MR using either deformable models, statistical models, or atlas-based segmentation, and a few studies have combined intensity and shape information. The combination of shape and intensity information might be used to achieve a more robust and more accurate segmentation compared with only using either intensity or shape information. Consequently, the two segmentation approaches presented in this thesis have combined intensity information and a level-set representation of the shape in an AAM addressed in Paper III and by combining atlas registration, intensity modeling, and graph cuts (AB+IM) addressed in Paper IV.

Validation of automatic segmentation is, as the case was for image registration, difficult as no ground truth segmentation exists. The most widely used validation approach is to compare the results with a manual delineation, as a manual delineation is the closest

to a ground truth possible though prone to e.g. interobserver variation [16, 17]. Both the AAM approach and the AB+IM approach were compared with manual prostate delineations originally used as the CTV. Thereby, the delineations were not intended to be used to build segmentation models or to validate prostate segmentations and the manual delineations might deviate from the prostate boundary, which all introduce an uncertainty in the validation of the segmentation approaches. The similarity metrics dice similarity coefficient (DSC) and mean surface distance (MSD) were used in both studies. The AB+IM approach was further compared with multi-atlas segmentation using majority labeling atlas fusion (AB) and by extending the AB+IM and AB with atlas selection.

The sensitivity and specificity of the AAM showed a trend towards undersegmentation of the large prostate volumes. This trend was also present for the AB and the AB+IM approaches without atlas selection. Although not validated on the same data sets, the findings indicate that the results might be improved by adding more data sets from patients with large prostates.

The AAM approach was validated on 30 data sets whereas the AB+IM approach was validation on 67 data sets. The data sets came from the same study conducted by Carl et al. [22] and therefore some of the data sets were used in both studies. However, this is not the case of the majority of the data set. Therefore, the results from the AAM and the AB+IM are difficult to compare, which could be met by using the same data sets for validation. The AB+IM approach was improved by an extension in form of atlas selection, which only keeps the atlases with the highest image similarity with the target image. The AAM uses all data sets to create a global model of the prostate shape and intensities.

The segmentation approaches have been validated on a data set from Aalborg University Hospital and a comparison of other prostate segmentation approaches is therefore difficult. A way to overcome this problem is to validate the approaches on data sets used for a MICCAI prostate segmentation challenge [61]. It will require a new training phase as the images from the challenge are acquired using an endorectal coil and the intensity distribution is not expected to be the same as the data sets used in the thesis.

Validation showed that an automatic segmentation might be used for CTV delineation as they, at least for the AB+IM approach, approached the inter-observer variation. Similar studies, which have performed prostate segmentation in MR, support the potentials of automatic segmentation approaches.

5.2 Future Work and Recommendations

In IGRT of prostate cancer further development is required to allow dose escalations and to reduce acute and long-term toxicities. One of the research areas is adaptive radiotherapy, which is a process where the treatment planning is modified between or during the treatment sessions, which may require multiple target contouring and multiple image registrations of MR and CT. This stresses the necessity of automatic registration and automatic segmentation as the manual labor is time-consuming and labor-intensive.

In this thesis, the CTV was defined as the prostate gland without the seminal vesicles. In high risk patients, the CTV includes the seminal vesicles as well as the prostate gland [98]. As a result, a natural next step would be to extend the AAM and AB+IM segmentation so that the seminal vesicles are included in the target. This extension is only needed

in high risk patients because a larger volume of the rectum, bladder etc. receives higher radiation dose with a risk of increasing the normal-tissue toxicity. The methods described in the thesis should easily be adapted to this purpose as well. However, it requires that a sufficient data set is available.

Another natural next step is to include the surrounding critical organs such as the rectum, the bladder, the trigone of urinary bladder, and the external anal sphincter, which are now all manually delineated. The AB+IM approach was extended by Fortunati et al. [94] to both include the critical tissues and the target for head and neck hyperthermia treatment and also an extension of the AAM is possible [99]. Alternatively, an extra step could be added to the methods, which aims to segment the other organs.

After a segmentation of the whole prostate gland, a further subdivision of the prostate in the central gland and the peripheral zone can be applied. Few studies have focused on this e.g. Toth et al. [99] using an AAM and Makni et al. [100] using both T2-weighted MR and diffusion weighted imaging in a C-means clustering algorithm. The subdivision of the prostate can be beneficial as approximately $70 - 80\%$ of all prostate tumors are located in the peripheral zone [101]. This permits that the treatment is tailored to the patient as the aggression of the cancer is location dependent and it may enable a radiation dose boost to the prostate zone, which contains the tumor. This will require that the tumor is accuratly localized.

5.3 Conclusion

This thesis has demonstrated the feasibility of the use of more automatic methods in the planning of radiotherapy of prostate cancer. Generic approaches used in previous studies were used throughout the thesis and adapted and evaluated to the specific aim of image registration and image segmentation of the prostate. For example the registration approach in the first study, which uses the widely used similarity measure mutual information in a two-step procedure to ensure an accurate alignment of the prostate in MR and CT. Therefore, it is reasonable to assume that the approach can work for other organs, which move relatively to the bone structures. Also, the segmentation approaches were adapted from [83, 84] and [93, 94] for the third study and fourth study, respectively. The segmentation approaches showed to be potential candidates for accurate target delineation in radiotherapy planning of prostate cancer. The work performed in the thesis is expected to be adaptable to target delineation of other organs, which can be described by a general shape and intensity distribution because of the segmentation methodologies.

References

[1] S. S. Ahmad, S. Duke, R. Jena, M. V. Williams, and N. G. Burnet, "Advances in radiotherapy." *BMJ*, vol. 345, no. dec04_1, p. e7765, 2012.

[2] L. A. Dawson and M. B. Sharpe, "Image-guided radiotherapy: rationale, benefits, and limitations." *Lancet Oncol.*, vol. 7, no. 10, pp. 848–858, 2006.

[3] L. A. Dawson and D. A. Jaffray, "Advances in image-guided radiation therapy." *J Clin Oncol*, vol. 25, no. 8, pp. 938–946, 2007.

[4] J. Staffurth, "A review of the clinical evidence for intensity-modulated radiotherapy." *Clin Oncol (R Coll Radiol)*, vol. 22, no. 8, pp. 643–657, 2010.

[5] M. K. Bucci, A. Bevan, and M. Roach, "Advances in Radiation Therapy: Conventional to 3D, to IMRT, to 4D, and Beyond," *CA Cancer J Clin*, vol. 55, no. 2, pp. 117–134, 2005.

[6] N. G. Burnet, S. J. Thomas, K. E. Burton, and S. J. Jefferies, "Defining the tumour and target volumes for radiotherapy." *Cancer Imaging*, vol. 4, no. 2, pp. 153–161, 2004.

[7] L. J. Boersma, M. van den Brink, A. M. Bruce, T. Shouman, L. Gras, A. te Velde, and J. V. Lebesque, "Estimation of the incidence of late bladder and rectum complications after high-dose (70-78 GY) conformal radiotherapy for prostate cancer, using dose-volume histograms." *Int J Radiat Oncol Biol Phys*, vol. 41, no. 1, pp. 83–92, 1998.

[8] D. A. Kuban, S. L. Tucker, L. Dong, G. Starkschall, E. H. Huang, M. R. Cheung, A. K. Lee, and A. Pollack, "Long-term results of the M. D. Anderson randomized dose-escalation trial for prostate cancer." *Int J Radiat Oncol Biol Phys*, vol. 70, no. 1, pp. 67–74, 2008.

[9] T. N. Eade, A. L. Hanlon, E. M. Horwitz, M. K. Buyyounouski, G. E. Hanks, and A. Pollack, "What dose of external-beam radiation is high enough for prostate cancer?" *Int J Radiat Oncol Biol Phys*, vol. 68, no. 3, pp. 682–689, 2007.

[10] W. D. Heemsbergen, A. Al-Mamgani, A. Slot, M. F. Dielwart, and J. V. Lebesque, "Long-term results of the Dutch randomized prostate cancer trial: Impact of dose-escalation on local, biochemical, clinical failure, and survival," *Radiother Oncol*, vol. 110, no. 1, pp. 104–109, 2014.

[11] G. L. Sannazzari, R. Ragona, M. G. Ruo Redda, F. R. Giglioli, G. Isolato, and A. Guarneri, "CT-MRI image fusion for delineation of volumes in three-dimensional conformal radiation therapy in the treatment of localized prostate cancer," *Br J Radiol*, vol. 75, no. 895, pp. 603–607, 2002.

[12] B. Hentschel, W. Oehler, D. Strauß, A. Ulrich, and A. Malich, "Definition of the CTV Prostate in CT and MRI by Using CT-MRI Image Fusion in IMRT Planning for Prostate Cancer," *Strahlenther Onkol*, vol. 187, no. 3, pp. 1–8, 2011.

[13] C. Rasch, I. Barillot, P. Remeijer, A. Touw, M. van Herk, and J. V. Lebesque, "Definition of the prostate in CT and MRI: a multi-observer study," *Int J Radiat Oncol Biol Phys*, vol. 43, no. 1, pp. 57–66, 1999.

[14] C. C. Parker, A. Damyanovich, T. Haycocks, M. Haider, A. Bayley, and C. N. Catton, "Magnetic resonance imaging in the radiation treatment planning of localized prostate cancer using intra-prostatic fiducial markers for computed tomography co-registration," *Radiother Oncol*, vol. 66, no. 2, pp. 217–224, 2003.

[15] M. De Brabandere, P. Hoskin, K. Haustermans, F. Van den Heuvel, and F.-A. Siebert, "Prostate post-implant dosimetry: interobserver variability in seed localisation, contouring and fusion." *Radiother Oncol*, vol. 104, no. 2, pp. 192–198, 2012.

[16] T. Nyholm, J. Jonsson, K. Söderström, P. Bergström, A. Carlberg, G. Frykholm, C. F. Behrens, P. F. Geertsen, R. Trepiakas, S. Hanvey, A. Sadozye, J. Ansari, H. McCallum, J. Frew, R. McMenemin, and B. Zackrisson, "Variability in prostate and seminal vesicle delineations defined on magnetic resonance images, a multi-observer, -center and -sequence study." *Radiat Oncol*, vol. 8, no. 1, p. 126, 2013.

[17] G. M. Villeirs, K. Van Vaerenbergh, L. Vakaet, S. Bral, F. Claus, W. J. De Neve, K. L. Verstraete, and G. O. De Meerleer, "Interobserver delineation variation using CT versus combined CT + MRI in intensity-modulated radiotherapy for prostate cancer." *Strahlenther Onkol*, vol. 181, no. 7, pp. 424–430, 2005.

[18] K. Langen and D. Jones, "Organ motion and its management," *Int J Radiat Oncol Biol Phys*, vol. 50, no. 1, pp. 265–278, 2001.

[19] M. S. Hoogeman, M. van Herk, J. de Bois, and J. V. Lebesque, "Strategies to reduce the systematic error due to tumor and rectum motion in radiotherapy of prostate cancer," *Radiother Oncol*, vol. 74, no. 2, pp. 177–185, 2005.

[20] J. M. Schallenkamp, M. G. Herman, J. J. Kruse, and T. M. Pisansky, "Prostate position relative to pelvic bony anatomy based on intraprostatic gold markers and electronic portal imaging," *Int J Radiat Oncol Biol Phys*, vol. 63, no. 3, pp. 800–811, 2005.

[21] V. Fonteyne, P. Ost, G. Villeirs, W. Oosterlinck, A. Impens, W. De Gersem, C. De Wagter, and G. De Meerleer, "Improving positioning in high-dose radiotherapy for prostate cancer: safety and visibility of frequently used gold fiducial markers." *Int J Radiat Oncol Biol Phys*, vol. 83, no. 1, pp. 46–52, 2012.

[22] J. Carl, J. Nielsen, M. Holmberg, E. H. Larsen, K. Fabrin, and R. V. Fisker, "A new fiducial marker for Image-guided radiotherapy of prostate cancer: clinical experience," *Acta Oncol*, vol. 47, no. 7, pp. 1358–1366, 2008.

[23] J. B. Thomsen, D. T. Arp, and J. Carl, "Urethra sparing - potential of combined nickel-titanium stent and intensity modulated radiation therapy in prostate cancer," *Radiother Oncol*, vol. 103, no. 2, pp. 256–260, 2012.

[24] J. Carl, J. Nielsen, M. Holmberg, E. H. Larsen, K. Fabrin, and R. V. Fisker, "Clinical results from first use of prostate stent as fiducial for radiotherapy of prostate cancer," *Acta Oncol*, vol. 50, no. 4, pp. 547–554, 2011.

[25] J. Maintz and M. A. Viergever, "A survey of medical image registration," *Med Image Anal*, vol. 2, no. 1, pp. 1–36, 1998.

[26] K. E. I. Deurloo, R. J. H. M. Steenbakkers, L. J. Zijp, J. A. de Bois, P. J. C. M. Nowak, C. R. N. Rasch, and M. van Herk, "Quantification of shape variation of prostate and seminal vesicles during external beam radiotherapy." *Int J Radiat Oncol Biol Phys*, vol. 61, no. 1, pp. 228–238, 2005.

[27] J. M. Hensel, C. Ménard, P. W. Chung, M. F. Milosevic, A. Kirilova, J. L. Moseley, M. A. Haider, and K. K. Brock, "Development of Multiorgan Finite Element-Based Prostate Deformation Model Enabling Registration of Endorectal Coil Magnetic Resonance Imaging for Radiotherapy Planning," *Int J Radiat Oncol Biol Phys*, vol. 68, no. 5, pp. 1522–1528, 2007.

[28] S. Vidakovic, H. S. Jans, A. Alexander, and R. S. Sloboda, "Post-implant computed tomography-magnetic resonance prostate image registration using feature line parallelization and normalized mutual information," *J Appl Clin Med Phys*, vol. 8, no. 1, pp. 21–32, 2006.

[29] H. J. Huisman, J. J. Fütterer, E. N. J. T. van Lin, A. Welmers, T. W. J. Scheenen, J. A. van Dalen, A. G. Visser, J. Witjes, and J. O. Barentsz, "Prostate Cancer: Precision of Integrating Functional MR Imaging with Radiation Therapy Treatment by Using Fiducial Gold Markers," *Radiology*, vol. 236, no. 1, pp. 311–317, 2005.

[30] O. Algan, G. E. Hanks, and A. H. Shaer, "Localization of the prostatic apex for radiation treatment planning." *Int J Radiat Oncol Biol Phys*, vol. 33, no. 4, pp. 925–930, 1995.

[31] K. Kagawa, W. R. Lee, T. E. Schultheiss, M. A. Hunt, A. H. Shaer, and G. E. Hanks, "Initial clinical assessment of CT-MRI image fusion software in localization of the prostate for 3D conformal radiation therapy," *Int J Radiat Oncol Biol Phys*, vol. 38, no. 2, pp. 319–325, 1997.

[32] A. Polo, F. Cattani, A. Vavassori, D. Origgi, G. Villa, H. Marsiglia, M. Bellomi, G. Tosi, O. D. Cobelli, and R. Orecchia, "MR and CT image fusion for postimplant analysis in permanent prostate seed implants," *Int J Radiat Oncol Biol Phys*, vol. 60, no. 5, pp. 1572–1579, 2004.

[33] J. Lian, L. Xing, S. Hunjan, C. Dumoulin, J. Levin, A. Lo, R. Watkins, K. Rohling, R. Giaquinto, D. Kim, D. Spielman, and B. Daniel, "Mapping of the prostate in endorectal coil-based mri/mrsi and ct: a deformable registration and validation study," *Med Phys*, vol. 31, no. 11, pp. 3087–3094, 2004.

[34] J. Crook, M. McLean, I. Yeung, T. Williams, and G. Lockwood, "MRI-CT fusion to assess postbrachytherapy prostate volume and the effects of prolonged edema on dosimetry following transperineal interstitial permanent prostate brachytherapy." *Brachytherapy*, vol. 3, no. 2, pp. 55–60, 2004.

[35] M. van Herk, J. C. de Munck, J. V. Lebesque, S. Muller, C. Rasch, and A. Touw, "Automatic registration of pelvic computed tomography data and magnetic resonance scans including a full circle method for quantitative accuracy evaluation," *Med Phys*, vol. 25, no. 10, pp. 2054–2067, 1998.

[36] F. Maes, D. Vandermeulen, and P. Suetens, "Medical image registration using mutual information," *Proceedings of the IEEE*, vol. 91, no. 10, pp. 1699–1722, 2003.

[37] P. W. McLaughlin, V. Narayana, M. Kessler, D. McShan, S. Troyer, L. Marsh, G. Hixson, and P. L. Roberson, "The use of mutual information in registration of CT and MRI datasets post permanent implant," *Brachytherapy*, vol. 3, no. 2, pp. 61–70, 2004.

[38] P. L. Roberson, P. W. McLaughlin, V. Narayana, S. Troyer, G. V. Hixson, and M. L. Kessler, "Use and uncertainties of mutual information for computed tomography/-magnetic resonance (CT/MR) registration post permanent implant of the prostate," *Med Phys*, vol. 32, no. 2, p. 473, 2005.

[39] D. Rueckert and J. A. Schnabel, "Medical Image Registration," *Biomedical Image Processing*, pp. 131–154, 2011.

[40] J. M. Fitzpatrick, D. L. G. Hill, Y. Shyr, J. West, C. Studholme, and C. R. M. Jr, "Visual assessment of the accuracy of retrospective registration of MR and CT images of the brain," *IEEE Trans Med Imaging*, vol. 17, no. 4, pp. 571–585, 1998.

[41] J. West, J. M. Fitzpatrick, M. Y. Wang, B. M. Dawant, C. R. Maurer, R. M. Kessler, R. J. Maciunas, C. Barillot, D. Lemoine, A. Collignon, F. Maes, P. Suetens, D. Vandermeulen, P. A. van den Elsen, S. Napel, T. S. Sumanaweera, B. Harkness, P. F. Hemler, D. L. Hill, D. J. Hawkes, C. Studholme, J. B. Maintz, M. A. Viergever, G. Malandain, and R. P. Woods, "Comparison and evaluation of retrospective intermodality brain image registration techniques." *J Comput Assist Tomogr*, vol. 21, no. 4, pp. 554–566, 1996.

[42] D. L. G. Hill, P. G. Batchelor, M. Holden, and D. J. Hawkes, "Medical image registration," *Phys Med Biol*, vol. 46, pp. R1–45, 2001.

[43] F. Maes, A. Collignon, D. Vandermeulen, G. Marchal, and P. Suetens, "Multimodality image registration by maximization of mutual information," *IEEE Trans Med Imaging*, vol. 16, no. 2, pp. 187–198, 1997.

[44] J. P. W. Pluim, J. B. A. Maintz, and M. A. Viergever, "Mutual-information-based registration of medical images: a survey," *IEEE Trans Med Imaging*, vol. 22, no. 8, pp. 986–1004, 2003.

[45] P. Viola and W. Wells, "Alignment by maximization of mutual information," in *Proceedings of IEEE International Conference on Computer Vision*. IEEE Comput. Soc. Press, 1995, pp. 16–23.

[46] A. Collignon, F. Maes, D. Delaere, D. Vandermeulen, P. Suetens, and G. Marchal, "Automated multi-modality image registration based on information theory," in *Information processing in medical imaging*, vol. 3, 1995, pp. 264–274.

[47] R. Graf, D. Boehmer, V. Budach, and P. Wust, "Interfraction rotation of the prostate as evaluated by kilovoltage x-ray fiducial marker imaging in intensity-modulated radiotherapy of localized prostate cancer," *Med Dosim*, vol. 37, no. 4, pp. 396–400, 2012.

[48] C. Noel, L. Santanam, J. Olsen, K. Baker, and P. Parikh, "An automated method for adaptive radiation therapy for prostate cancer patients using continuous fiducial-based tracking," *Phys Med Biol*, vol. 55, no. 1, pp. 65–82, 2010.

[49] Q. Shang, L. J. Sheplan Olsen, K. Stephans, R. Tendulkar, and P. Xia, "Prostate rotation detected from implanted markers can affect dose coverage and cannot be simply dismissed." *J Appl Clin Med Phys*, vol. 14, no. 3, pp. 177–191, 2013.

[50] I. M. Lips, U. A. van der Heide, A. N. Kotte, M. van Vulpen, and A. Bel, "Effect of Translational and Rotational Errors on Complex Dose Distributions With Off-Line and On-Line Position Verification," *Int J Radiat Oncol Biol Phys*, vol. 74, no. 5, pp. 1600–1608, 2009.

[51] J.-F. Aubry, L. Beaulieu, L.-M. Girouard, S. Aubin, D. Tremblay, J. Laverdière, and E. Vigneault, "Measurements of intrafraction motion and interfraction and intrafraction rotation of prostate by three-dimensional analysis of daily portal imaging with radiopaque markers." *Int J Radiat Oncol Biol Phys*, vol. 60, no. 1, pp. 30–39, 2004.

[52] E. Huang, L. Dong, A. Chandra, D. A. Kuban, I. I. Rosen, A. Evans, and A. Pollack, "Intrafraction prostate motion during IMRT for prostate cancer." *Int J Radiat Oncol Biol Phys*, vol. 53, no. 2, pp. 261–268, 2002.

[53] J. Carl, B. Lund, E. H. Larsen, and J. Nielsen, "Feasibility study using a Ni-Ti stent and electronic portal imaging to localize the prostate during radiotherapy," *Radiother Oncol*, vol. 78, no. 2, pp. 199–206, 2006.

[54] D. L. Collins, P. Neelin, T. M. Peters, and A. C. Evans, "Automatic 3D intersubject registration of MR volumetric data in standardized Talairach space," *J Comput Assist Tomogr*, vol. 18, no. 2, pp. 192–205, 1994.

[55] McConnell Brain Imaging Center., "Minctracc help page." [Online]. Available: http://www.bic.mni.mcgill.ca/~dale/helppages/mni_man/minctracc.html

[56] L. Dice, "Measures of the amount of ecologic association between species," *Ecology*, vol. 26, pp. 297–302, 1945.

[57] L. Sander, N. C. Langkilde, M. Holmberg, and J. Carl, "MRI target delineation may reduce long-term toxicity after prostate radiotherapy." *Acta Oncol*, 2013.

[58] D. L. Pham, C. Xu, and J. L. Prince, "Current methods in medical image segmentation." *Annu Rev Biomed Eng*, vol. 2, pp. 315–337, 2000.

[59] T. Heimann and H.-P. Meinzer, "Statistical shape models for 3D medical image segmentation: a review." *Med Image Anal*, vol. 13, no. 4, pp. 543–63, 2009.

[60] S. Ghose, A. Oliver, R. Martí, X. Lladó, J. C. Vilanova, J. Freixenet, J. Mitra, D. Sidibé, and F. Meriaudeau, "A survey of prostate segmentation methodologies in ultrasound, magnetic resonance and computed tomography images," *Comput Methods Programs Biomed*, vol. 108, no. 1, pp. 262–287, 2012.

[61] G. Litjens, R. Toth, W. van de Ven, C. Hoeks, S. Kerkstra, B. van Ginneken, G. Vincent, G. Guillard, N. Birbeck, J. Zhang, R. Strand, F. Malmberg, Y. Ou, C. Davatzikos, M. Kirschner, F. Jung, J. Yuan, W. Qiu, Q. Gao, P. E. Edwards, B. Maan, F. van der Heijden, S. Ghose, J. Mitra, J. Dowling, D. Barratt, H. Huisman, and A. Madabhushi, "Evaluation of prostate segmentation algorithms for MRI: The PROMISE12 challenge," *Med Image Anal*, vol. 18, no. 2, pp. 359–373, 2014.

[62] D. Flores-Tapia, N. Venugopal, G. Thomas, B. McCurdy, L. Ryner, and S. Pistorius, "Real time mri prostate segmentation based on wavelet multiscale products flow tracking," in *Conf Proc IEEE Eng Med Biol Soc*. IEEE, 2010, pp. 5034–5037.

[63] R. Zwiggelaar, Y. Zhu, and S. Williams, "Semi-automatic segmentation of the prostate," *Pattern Recognition and Image Analysis*, pp. 1108–1116, 2003.

[64] S. Ghose, J. Mitra, A. Oliver, R. Marti, X. Lladó, J. Freixenet, J. C. Vilanova, D. Sidibé, and F. Meriaudeau, "Graph cut energy minimization in a probabilistic learning framework for 3d prostate segmentation in mri," in *ICPR*, 2012, pp. 125–128.

[65] S. Martin, V. Daanen, and J. Troccaz, "Atlas-based prostate segmentation using an hybrid registration," *Int J Comput Assist Radiol Surg*, vol. 3, no. 6, pp. 485–492, 2008.

[66] M. Cabezas, A. Oliver, X. Lladó, J. Freixenet, and M. B. Cuadra, "A review of atlas-based segmentation for magnetic resonance brain images," *Comput Methods Programs Biomed*, vol. 104, no. 3, pp. e158–e177, 2011.

[67] S. Klein, U. A. van der Heide, I. M. Lips, M. van Vulpen, M. Staring, and J. P. W. Pluim, "Automatic segmentation of the prostate in 3D MR images by atlas matching using localized mutual information," *Med Phys*, vol. 35, no. 4, pp. 1407–1417, 2008.

[68] J. Dowling, J. Fripp, S. Chandra, J. Pluim, J. Lambert, J. Parker, J. Denham, P. Greer, and O. Salvado, "Fast automatic multi-atlas segmentation of the prostate from 3d mr images," *Prostate Cancer Imaging. Image Analysis and Image-Guided Interventions*, pp. 10–21, 2011.

[69] T. R. Langerak, U. A. van der Heide, A. N. T. J. Kotte, M. A. Viergever, M. van Vulpen, and J. P. W. Pluim, "Label fusion in atlas-based segmentation using a selective and iterative method for performance level estimation (simple)," *IEEE Trans Med Imaging*, vol. 29, no. 12, pp. 2000–2008, 2010.

[70] T. R. Langerak, F. F. Berendsen, U. A. Van der Heide, A. N. T. J. Kotte, and J. P. W. Pluim, "Multiatlas-based segmentation with preregistration atlas selection," *Med Phys*, vol. 40, no. 9, p. 091701, 2013.

[71] S. Martin, J. Troccaz, and V. Daanen, "Automated segmentation of the prostate in 3d mr images using a probabilistic atlas and a spatially constrained deformable model," *Med Phys*, vol. 37, no. 4, pp. 1579–1590, 2010.

[72] S. Chandra, J. Dowling, K.-K. Shen, P. Raniga, J. Pluim, P. Greer, O. Salvado, and J. Fripp, "Patient specific prostate segmentation in 3-d magnetic resonance images," *IEEE Trans Med Imaging*, vol. 31, no. 10, pp. 1955 –1964, 2012.

[73] D. Pasquier, T. Lacornerie, M. Vermandel, J. Rousseau, E. Lartigau, and N. Betrouni, "Automatic segmentation of pelvic structures from magnetic resonance images for prostate cancer radiotherapy," *Int J Radiat Oncol Biol Phys*, vol. 68, no. 2, pp. 592–600, 2007.

[74] N. Makni, P. Puech, R. Lopes, A. S. Dewalle, O. Colot, and N. Betrouni, "Combining a deformable model and a probabilistic framework for an automatic 3D segmentation of prostate on MRI." *Int J Comput Assist Radiol Surg*, vol. 4, no. 2, pp. 181–188, 2009.

[75] N. Chowdhury, R. Toth, J. Chappelow, S. Kim, S. Motwani, S. Punekar, H. Lin, S. Both, N. Vapiwala, S. Hahn, and Others, "Concurrent segmentation of the prostate on MRI and CT via linked statistical shape models for radiotherapy planning," *Med Phys*, vol. 39, no. 4, pp. 2214–2228, 2012.

[76] N. Chowdhury, J. Chappelow, R. Toth, S. Kim, S. Hahn, N. Vapiwala, H. Lin, S. Both, and A. Madabhushi, "Linked statistical shape models for multi-modal segmentation of the prostate on mri-ct for radiotherapy planning," in *Proc. of SPIE Vol*, vol. 7963, 2011, pp. 796 314–796 311.

[77] A. Tsai, A. Yezzi, W. Wells, C. Tempany, D. Tucker, A. Fan, W. E. Grimson, and A. Willsky, "A shape-based approach to the segmentation of medical imagery using level sets." *IEEE Trans Med Imaging*, vol. 22, no. 2, pp. 137–154, 2003.

[78] R. Toth and A. Madabhushi, "Multifeature landmark-free active appearance models: Application to prostate mri segmentation," *IEEE Trans Med Imaging*, vol. 31, no. 8, pp. 1638–1650, 2012.

[79] S. Ghose, A. Oliver, R. Marti, X. Lladó, J. Freixenet, J. C. Vilanova, and F. Meriaudeau, "Prostate segmentation with texture enhanced active appearance model," in *2010 Sixth International Conference on Signal-Image Technology and Internet-Based Systems (SITIS)*. IEEE, 2010, pp. 18–22.

[80] T. F. Cootes, C. J. Taylor, D. H. Cooper, and J. Graham, "Active shape models-their training and application," *Computer Vision and Image Understanding*, vol. 61, no. 1, pp. 38–59, 1995.

[81] T. F. Cootes, G. J. Edwards, and C. J. Taylor, "Active appearance models," *Computer Vision ECCV 98*, vol. 23, no. 6, pp. 681–685, 1998.

[82] ——, "Active appearance models," *IEEE Trans Pattern Anal Mach Intell*, vol. 23, no. 6, pp. 681–685, 2001.

[83] S. Hu and D. L. Collins, "Joint level-set shape modeling and appearance modeling for brain structure segmentation," *NeuroImage*, vol. 36, no. 3, pp. 672–683, 2007.

[84] U. L. Stephansen, "Level-set appearance modeling for segmentation of anatomical structures in 3-D images," Tech. Rep., 2012.

[85] T. F. Cootes and C. J. Taylor, "Statistical models of appearance for computer vision," *Imaging Science and Biomedical Engineering, University of Manchester, Manchester M13 9PT, UK March*, vol. 8, 2004.

[86] M. Leventon, W. Grimson, and O. Faugeras, "Statistical shape influence in geodesic active contours," in *Proceedings IEEE Conference on Computer Vision and Pattern Recognition. CVPR 2000*, vol. 1. IEEE Comput. Soc, 2000, pp. 316–323.

[87] G. Borgefors, "Another comment on "a note on 'distance transformations in digital images' "," in *CVGIP: Image Understanding*, vol. 54, no. 2, 1991, pp. 301–306.

[88] N. Betrouni, A. Iancu, P. Puech, S. Mordon, and N. Makni, "ProstAtlas: a digital morphologic atlas of the prostate." *Eur J Radiol*, vol. 81, no. 9, pp. 1969–1975, 2012.

[89] M. Rusu, B. N. Bloch, C. C. Jaffe, N. M. Rofsky, E. M. Genega, E. Feleppa, R. E. Lenkinski, and A. Madabhushi, "Statistical 3D prostate imaging atlas construction via anatomically constrained registration," in *SPIE Medical Imaging*. International Society for Optics and Photonics, Mar. 2013, pp. 866 913–866 913–9.

[90] J. M. Lötjönen, R. Wolz, J. R. Koikkalainen, L. Thurfjell, G. Waldemar, H. Soininen, and D. Rueckert, "Fast and robust multi-atlas segmentation of brain magnetic resonance images." *NeuroImage*, vol. 49, no. 3, pp. 2352–2365, 2010.

[91] S. Klein, M. Staring, K. Murphy, M. A. Viergever, and J. P. Pluim, "Elastix: a toolbox for intensity-based medical image registration," *IEEE Trans Med Imaging*, vol. 29, no. 1, pp. 196–205, 2010.

[92] P. Aljabar, R. A. Heckemann, A. Hammers, J. V. Hajnal, and D. Rueckert, "Multi-atlas based segmentation of brain images: atlas selection and its effect on accuracy." *NeuroImage*, vol. 46, no. 3, pp. 726–738, 2009.

[93] F. van der Lijn, T. den Heijer, M. Breteler, and W. J. Niessen, "Hippocampus segmentation in mr images using atlas registration, voxel classification, and graph cuts." *NeuroImage*, vol. 43, no. 4, pp. 708–720, 2008.

[94] V. Fortunati, R. F. Verhaart, F. van der Lijn, W. J. Niessen, J. F. Veenland, M. M. Paulides, and T. van Walsum, "Tissue segmentation of head and neck CT images for treatment planning: A multiatlas approach combined with intensity modeling," *Med Phys*, vol. 40, no. 7, p. 071905, 2013.

[95] S. Kumar and M. Hebert, "Discriminative random fields: A discriminative framework for contextual interaction in classification," in *Ninth IEEE International Conference on Computer Vision, 2003. Proceedings.* IEEE, 2003, pp. 1150–1157.

[96] V. Kolmogorov and R. Zabih, "What energy functions can be minimized via graph cuts?" *IEEE Trans Pattern Anal Mach Intell*, vol. 26, no. 2, pp. 147–159, 2004.

[97] Y. Boykov and V. Kolmogorov, "An experimental comparison of min-cut/max-flow algorithms for energy minimization in vision," *IEEE Trans Pattern Anal Mach Intell*, vol. 26, no. 9, pp. 1124–1137, 2004.

[98] L. L. Kestin, N. S. Goldstein, F. A. Vicini, D. Yan, H. J. Korman, and A. A. Martinez, "Treatment of prostate cancer with radiotherapy: should the entire seminal vesicles be included in the clinical target volume?" *Int J Radiat Oncol Biol Phys*, vol. 54, no. 3, pp. 686–697, 2002.

[99] R. Toth, J. Ribault, J. Gentile, D. Sperling, and A. Madabhushi, "Simultaneous segmentation of prostatic zones using Active Appearance Models with multiple coupled levelsets," *Computer Vision and Image Understanding*, vol. 117, no. 9, pp. 1051–1060, 2013.

[100] N. Makni, A. Iancu, O. Colot, P. Puech, S. Mordon, and N. Betrouni, "Zonal segmentation of prostate using multispectral magnetic resonance images," *Med Phys*, vol. 38, no. 11, pp. 6093–6105, 2011.

[101] E. Niaf, O. Rouvière, F. Mège-Lechevallier, F. Bratan, and C. Lartizien, "Computer-aided diagnosis of prostate cancer in the peripheral zone using multiparametric MRI." *Phys Med Biol*, vol. 57, no. 12, pp. 3833–3851, 2012.

Contributions

Paper I

MR-CT Registration using a Ni-Ti Prostate Stent in Image-Guided Radiotherapy of Prostate Cancer

Anne Sofie Korsager, Jesper Carl, and Lasse Riis Østergaard

This appendix is based on a paper published in:
Medical Physics, Vol. 40, No. 6, 2013

A part of this thesis has been removed from this publication due to copyright.

Paper II

Comparison of manual and automatic MR-CT image registration for image-guided radiotherapy of prostate cancer

Anne Sofie Korsager, Jesper Carl, and Lasse Riis Østergaard

This appendix is based on a paper submitted

A part of this thesis has been removed from this publication due to copyright.

Paper III

The use of an Active Appearance Model for Automated Prostate Segmentation in Magnetic Resonance

Anne Sofie Korsager, Ulrik Landberg Stephansen, Jesper Carl, and Lasse Riis Østergaard

This appendix is based on a paper published in:
Acta Oncologica

A part of this thesis has been removed from this publication due to copyright.

Paper IV

The use of Atlas Registration and Graph Cuts for Prostate Segmentation in Magnetic Resonance Images

Anne Sofie Korsager, Valerio Fortunati, Fedde van der Lijn, Jesper Carl, Wiro Niessen, Lasse Riis Østergaard, and Theo van Walsum

This appendix is based on a paper submitted

A part of this thesis has been removed from this publication due to copyright.